A Magnetically Controllable Valve to Vary the Resistance of Hydraulic Dampers in Exercise Equipment

A Dissertation Submitted to the Graduate Faculty of

Baylor University

in Partial Fulfillment of the

Requirements for the Degree

of

Master of Science

By

Brett M. Levins

Waco, Texas

August 2005

TABLE OF CONTENTS

LIST OF FIGURES

LIST OF ABBREVIATIONS

x	magnetic valve gap; the gap between the magnet and the piston head
A_{in}	fluid inlet orifice area (constant)
A_{out}	fluid outlet orifice area (constant)
A_p	area of piston head (constant)
A_{max}	max effective fluid orifice area (constant)
$A(x)$	measured effective fluid orifice area
$\hat{A}(x)$	projected effective fluid orifice area
f_{flu}	force of fluid exerted on valve
f_{mag}	magnetic force exerted on valve
f_{gas}	gas accumulator force exerted on piston
ΔP	pressure difference across piston
F	force developed by damper
ρ	fluid mass density (constant)
k	adjustment to Bernoulli's equation (constant)
v_p	velocity of piston
$Q(x)$	stiffness of damper
Q_{min}	minimum stiffness of damper
$g(x)$	fluid force modulation function
o_d	orifice diameter (constant)
I	applied current

ACKNOWLEDGMENTS

I would like to thank Dr. Ian Gravagne for his exceptional teaching and guidance throughout my research at Baylor University. Also, I am grateful for a grant from Curves International (contract 097-04-Curves) to fuel my research. Finally, I would like to show appreciation to Ashley Orr and Blake Branson for technical assistance in construction and assembly of the dampers.

DEDICATION

To my parents, whose constant support continues to be my motivation.

CHAPTER ONE

Introduction

It has become quite noticeable in recent years that linear fluid damping can be utilized as an effective and economical way to provide resistance for exercise machines. Linear dampers have numerous advantages to recent counterparts such as weights and resistance bands. Dampers are small and compact, unlike commonly employed resistance devices that need cables and pulleys to provide resistance. Also, fluid dampers are mass produced for the automotive industry, leaving them inexpensive and easy to obtain. The most observable advantage over other types of resistances, however, is the ability to provide resistance in both compression and extension (both directions of the stroke), often referred to as "double positive" resistance. Exercise machine designers can utilize linear dampers to provide exercise to several different muscle groups on the same machine. This is highly beneficial to exercise companies that wish to provide circuit training with a small number of machines. In addition to smaller numbers of machines, dampers aesthetically provide exercise equipment with an appearance that is not overwhelming; a positive for many beginner exercisers who may be discouraged from a complex weight and pulley system.

Despite the fact that linear dampers have many advantages, they do have one disadvantage: they are difficult to adjust. Adjustability, though sometimes found on pneumatic dampers, is rarely found on fluid dampers due to the fact that fluid dampers must remain sealed at all times and do not have the ability to draw in or release air from the damper. There has been research into linear dampers not based on fluid or gas [5][9],

but without the damping effect of fluid, energy must be dissipated through the active element of the design. This active element is commonly an electromagnet or a motor, and tends to increase the size and complexity of the device.

In the past, the fluid adjustability problem has been remedied in two different ways. The first solution is to physically change the size of the orifice using a knob or similar device. This technique is commonly used in gas dampers, but not in fluid dampers. Since fluid dampers need to be completely sealed to prevent air from entering the system, it is difficult to design dampers with mechanical fixtures that do not jeopardize the damper seal. It is also possible to adjust orifice sizes within the cylinder by controlling a valve using different types of motors. This valve controlling tends to add complexity to the system and requires feedback from the motor, leaving the damper difficult to control.

Conversely, the second way to control a fluid damper is to actually change the viscous properties of the fluid itself. Recently, the use of magnetorheological (MR) and electrorheological (ER) fluids have increased in damper design [1] [2] [4] [6] [7]. These fluids have the ability to become more viscous upon the application of a magnetic or electric field, thus dynamically adjusting the resistance of the damper depending on the strength of the field. These types of dampers appear to be the best choice, but the high cost of the fluid leaves the dampers as a non-economical solution to many exercise companies. Each of these control designs will be examined in more depth later.

The author was approached by an exercise company providing guidelines to the development of an adjustable damper that gave purpose to this thesis. An adjustable damper needed to be developed for the use in exercise equipment that would effectively

change resistances to accommodate for a wide force range. The damper needed to be a simple design that would be easy to maintain, and also have the ability to be mass produced at a minimal cost. The author decided that the most suitable way to control the strength of the damper at a minimal cost would be to design for an internal variable orifice. This thesis presents a damper design that will control orifice size in an unconventional manner. The damper utilizes two electromagnets and their repulsive magnetic field to block and control the size of an orifice by creating a magnetic valve. The author presents a hypothesis of the behavior of the magnetic valve suggesting how the effective orifice area on the piston head is related to the gap distance between the magnet and the piston head. Using a developed testing platform, force-velocity tests have been performed and presented to describe the characteristics of two constructed cylinders. Finally, the force-velocity characteristics of the developed dampers are exhibited and analyzed for a range of applied currents to the electromagnets.

CHAPTER TWO

Current Adjustable Dampers

Magnetorheological and Electrorheological Fluids

As mentioned earlier, there are currently two different ways to dynamically control the resistance of a fluid damper. The most popular way is to incorporate MR or ER fluid into the cylinder. MR fluid consists of a base fluid, usually hydraulic oil, and suspended particles of iron randomly dispersed within the fluid. When a magnetic field is applied across the fluid, the iron particles line up and create "chains" along the magnetic field lines. These chains, in turn, resist the flow of the fluid. The strength of the chains, and resulting flow resistance, depends on the strength of the magnetic field [4]. Similarly, ER fluids also consist of a base fluid and suspended particles. They differ from MR fluids in that the particles form chains when an electric field is applied directly to the fluid itself. Both fluids have proven to be exceptionally strong and have large bandwidths. MR fluids are known to resist pressures of 50-100 kPa at maximum magnetic field strengths of 250 kA/m, while ER fluids can resist pressures of 2-5 kPa at electric field strengths of up to 4 kV/mm [10]. The large voltages that ER fluids require tend to guide engineers to the use of the more manageable MR fluids. The main problem with MR and ER fluids is the fact that they begin to break down over time. This phenomenon is known as "in-use thickening [11]." When an ER or MR fluid is subjected to high shear stresses for a significant period of time, the fluid begins to thicken until it eventually becomes unmanageable. In typical exercise machines, it is projected that a damper will incur a million strokes per year and needs the ability to last around three to five years. Currently

produced MR and ER fluids have the ability to withstand these numbers of strokes, but only when high priced agents are added to the fluid. This high price (around $100 per US liter) leaves MR or ER fluid as a bad economical choice for exercise equipment. Additionally, the agents added to commercially produced fluid not only improve the lifetime of the fluid, but also reduce the unavoidable problem of particle settlement. For this reason, simpler MR or ER fluids are unable to be developed for this application due to the fact that the particles will begin to settle between uses of the equipment.

In order to avoid the use of excessive volumes of MR fluids in dampers (and associated extra cost), MR sponge devices have been developed and implemented in certain applications [2]. MR sponges consist of a piston head with an electromagnet covered with a sponge like material that has been soaked in MR fluid. Once current is applied to the electromagnet, the MR sponge on the piston head acts in direct-shear mode with the piston wall. This is in contrast to the pressure driven flow mode MR fluid experiences when flowing through an orifice [4]. Since the MR fluid is soaked into the sponge device on the piston head, no fluid is needed inside the damper. Therefore, the damper can function with air in the volume usually occupied by the base oil of damper. The smaller amount of MR fluid significantly lowers the cost of the damper. MR fluid sponge devices were developed and tested for application in this project. Although the cost of the damper was manageable for large scale production, necessary force levels for use in exercise equipment could not be reached by the developed MR sponge dampers.

Restrictive Orifice Designs

A second way to change a damper's resistance is to restrict the size of the orifice either externally or internally. External control of an adjustable orifice typically consists

of a knob on the outside of the damper that dynamically controls the size of the orifice. The knob can be turned to open or close the orifice with the precision of the change in orifice size depending on the thread size of the knob. This type of design is usually only implemented on air dampers due to the importance of sealing fluid dampers [3]. Also, external control is often awkward and time-consuming to change, another disadvantage for exercise machines. Fluid dampers with mechanical adjustments are rarely used in exercise equipment; refer to [8] for an implementation for this type of damper.

Internal control of orifice size is usually accomplished by a motor-like device on the piston head that has the ability to block an orifice. These types of constructions are beneficial because they are completely contained within the cylinder and have shown to work relatively well. The main problem with motor type designs is that they require feedback for the controller. Feedback often complicates systems and requires extra hardware for control. The more control that is needed for the system, the more expensive the system becomes.

CHAPTER THREE

Presented Adjustable Damper Model

An adjustable damper focusing on a simple design has been developed and is presented in the following chapter. Work described and presented in this paper closely follows work presented by Levins and Gravagne [12].

Description of Simple Damper

Before analyzing how the presented damper works, we must first understand, in general, how a typical damper works. A simple damper consists of two volumes of fluid separated by a piston head that contains an orifice (a hole smaller than the diameter of the piston head that allows fluid to flow between the two volumes). Upon moving either direction, a pressure differential is created between the two volumes and causes the fluid to flow through the orifice in order to equal the pressure once again. Since the area of the orifice is smaller, usually significantly smaller, than the area of the piston head, the movement of the piston head is hampered. This hampering of the piston head is often referred to as inertial damping. Imagine a small mass of fluid on the high pressure fluid volume. The small mass is forced from the high pressure volume into the orifice. Since the orifice contains significantly less volume than the original fluid volume, the mass will travel at a faster velocity while inside the orifice. Once the mass travels through the orifice and reaches the larger fluid volume on the other side of the piston, the mass will once again slow down. This process of speeding up and then slowing down causes the damping effect “felt” in the damper.

The amount of force required to displace a piston head at a given velocity for a simple orifice is shown in figure 1. Note that the force-velocity (FV) curve for an orifice is quadratic with the stiffness increasing as the size of the orifice becomes smaller. The fact that the faster a damper moves, the harder it becomes is beneficial to exercise equipment. This helps to account for a wide range of user strengths on an exercise machine. If a stronger exerciser is on the machine, they can simply move the damper faster and obtain the force levels they need out of the damper.

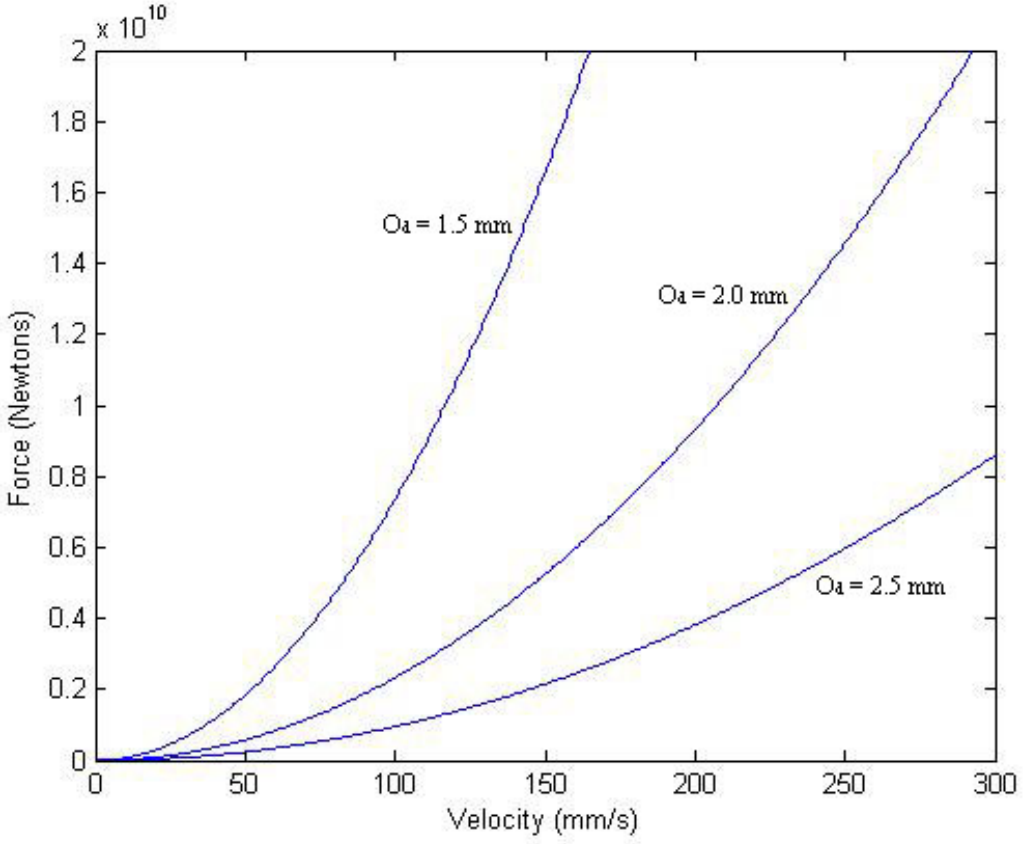

Figure 1: Sample Orifice Sizes for Simple Piston Head – The force-velocity characteristics of a simple damper and piston head for 3 different orifice sizes. The plot demonstrates the fact that as orifice sizes begin to decrease, the damper becomes stiffer.

However, exercising at faster speeds begins to create more of an aerobic workout than a strength workout, a non-ideal result for some exercise companies. Therefore, a damper that can control the size of the orifice on the piston head would be beneficial in order to account for a range of strength for different exercisers.

Description of Presented Damper

The presented damper model is shown below in figure 2. The damper consists of three main chambers: a magnet chamber and two fluid chambers. The two fluid chambers are represented by the volume of fluid in the chamber, V_A and V_B. The magnet chamber is located between two piston heads, Piston A and Piston B, which are roughly 10 cm apart and divide the fluid volumes from the magnet chamber. A gas accumulator is included within the piston in order to account for the difference in volume created by the piston rod during a stroke.

The piston heads consist of one orifice and a check valve that allows fluid to only flow from within the magnet chamber to the fluid chamber. The orifices on each piston head are equipped with a rubber washer on the magnet chamber side to guarantee that there is a strong seal between the associated magnet and piston head. Each piston head contains a Teflon seal between the piston head and the inside wall of the damper to ensure all fluid must travel through the orifice or check valve instead of escaping around the sides of the piston head. Inside the magnet chamber are two electromagnets, Magnet A and Magnet B, that are capable of sliding separately and without restraint on a steel shaft. Once excited, the magnets are oppositely poled and consequently repel each other, creating a small gap between the two.

During an extension stroke, a static pressure difference is created between V_A and V_B. This pressure difference causes fluid to flow from V_A through the orifice on Piston A into the magnet chamber. In order for this to happen, Magnet A must displace off of Piston A to allow the fluid to enter the magnet chamber. The entering fluid then exits out of the check valve on Piston B. Note that Magnet B is blocking and sealing the orifice on Piston B, therefore all the exiting fluid must travel through the check valve. This process is reversed for a compression stroke. Fluid travels into the orifice on Piston B, through the magnet chamber, and out of the check valve on Piston A. Figures 3 and 4 show an up close version of the conceptual design of the piston head assembly and the actual construction of the piston head assembly, respectively.

Analysis of the Magnetic Valve

Understanding the way in which a magnet interacts with the orifice on the piston head is crucial to the analysis of this damper. Jets of fluid flowing through the orifice on the piston head strike the face of the magnet upon entering the magnet chamber. The magnet on the high pressure side of the piston head acts as a valve in which the gap between the magnet and the piston head controls how much fluid is entering the magnet chamber. The valve controls how much fluid is entering the magnet chamber by restraining the area of the inlet orifice, A_{in}. Therefore, A_{in} is controlled by the strength of the magnetic field (the controlling factor on the gap size). However, there is a maximum rate that fluid can enter the magnet chamber which depends solely on the maximum area of the orifice, A_{max}; a value determined by the orifice diameter. Imagine spraying water from a hose against a brick wall. As the spray becomes closer to the wall, the exiting water feels more forceful against the wall. A common way to re-create that same close

proximity force would be to back up from the wall and obstruct the outlet of the hose. This obstruction has created a smaller orifice. This implies a correlation involving the gap size between an orifice and an impeding structure, and the effective size of that orifice.

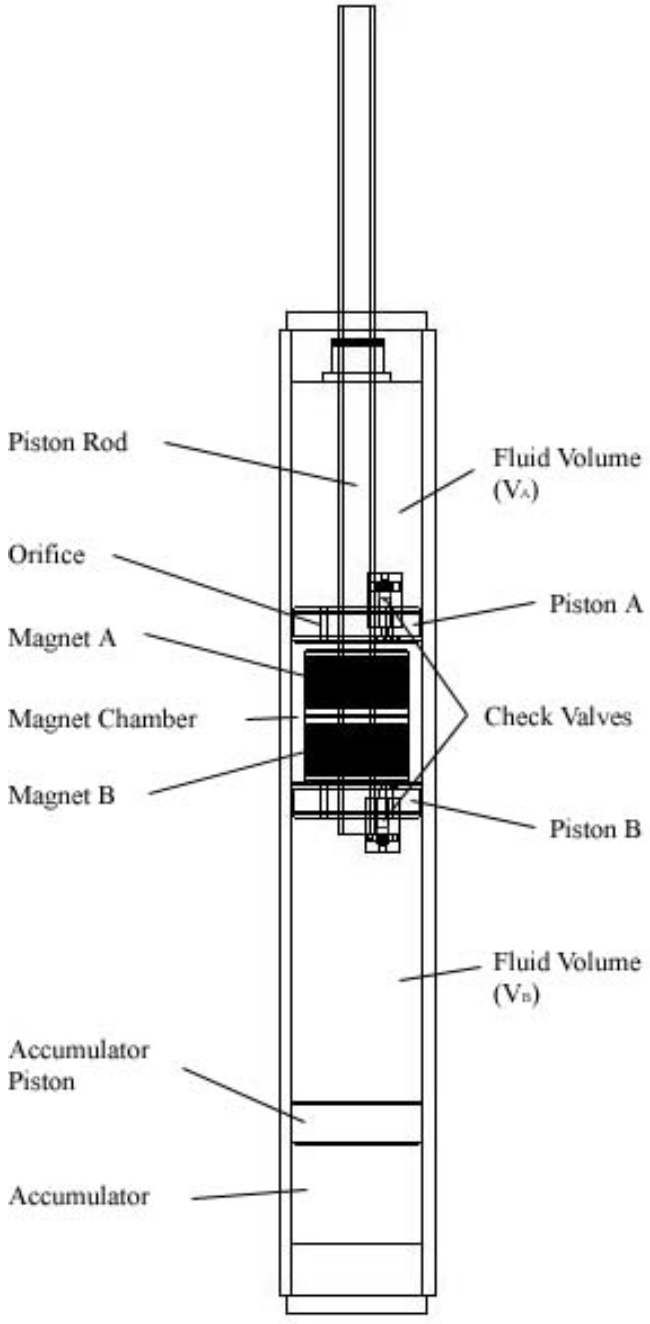

Figure 2: Presented Damper Diagram – A diagram of the presented damper body and valve. The remote reservoir of the system is represented by the accumulator in this figure for demonstration purposes.

Figure 3: Conceptual Valve Assembly – The conceptual design of the magnetic valve when the 2 electromagnets are at rest. If excited with current, the gap would be visible between the magnets.

Figure 4: Actual Piston Assembly – A close-up of the magnetic valve on the piston heads after it has been constructed.

In the presented damper design, the piston head consists of a single orifice and a check valve. The check valve is significantly larger than the orifice to allow the FV characteristics of the damper to be dependant on the orifice size alone. Therefore, the orifice shows a maximum inlet area A_{max} of,

$$A_{\max} = \pi\left(\frac{o_d}{2}\right)^2 \tag{1}$$

where o_d is the orifice diameter.

Now, let x(t) represent the gap between the piston head and the magnet $(0 \le x \le 1.4mm)$, m be the mass of the magnet, and b the fluid damping constant. While in motion, the fluid force exerted onto the magnet, f_{flu}, must equal the magnetic field force, f_{mag}, as

$$m\ddot{x} + b\dot{x} - f_{flu} + f_{mag} = 0 \tag{2}$$

The magnetic force, f_{mag}, is controlled by the applied current I. Therefore, since the magnets essentially adjust the size of the orifice, the presented damper becomes dynamically adjustable depending on the amount of current that is applied to the magnets. Increasing currents will create a stronger repulsive magnetic field between the magnets which, in turn, will allow the magnets to resist a larger force from the fluid trying to enter into the magnet chamber. An interpretation of this would be that the magnet is "shrinking" the size of the orifice. Also, since the values of x stay below 1mm, the design takes advantage of the fact that the strength of opposing magnetic fields increase exponentially as two magnets become closer in proximity. The small x values are also beneficial because this leaves $f_{mag}(I)$ independent to the value of x. On the other

hand, f_{flu} is a function of x and the differential pressure across the piston head, $\Delta P = P_B - P_A$.

The formulation of $f_{flu}(x, \Delta P)$ begins to become complex because it must capture the transition from a pure reaction force (when $x = 0$ and f_{flu} is only dependant on the pressure) to an impulse force (when the jets of fluid from the orifice impinge on the face of the magnet as the gap opens). This implies that f_{flu} depends on the velocity of the fluid jets; furthermore, the fluid jet velocity depends on the effective orifice size and the differential pressure across the piston head. Therefore, it is observed that

$$f_{flu} = \Delta P A_{\max} g(x) \tag{3}$$

with the arbitrary function $g(x) \le 1$. It is beyond the scope of the thesis to fully investigate the function $g(x)$. Now we turn our attention to the effective orifice area as a function of the gap, x.

Since the acting magnetic valve only changes the effective orifice size, Bernoulli's equation supplies the suitable relationship. Now, let $A(x)$ be the effective orifice area of the piston head, noting that $A(x) \to A_{\max}$ as $x \to \infty$. Also, if we assign the piston head area to be A_p and assume that the cross-sectional area of the piston rod is small compared to the area of the piston face, Bernoulli's equation gives

$$\Delta P = \frac{\rho A_p^2}{2k^2 A(x)^2} v_p^2 \tag{4}$$

In true laminar flows, the constant k would equal 1, although in practice it lies in the range of 0.8 to 0.9 [3]. The force of the damper is related to the ΔP of the system by the aggregate damper force, $F = \Delta P A_p$. Also, when relating the velocity to the force, two

additional cylinder effects arise: the velocity-dependent friction of piston head and rod when sliding within their respective seals, and the force exerted by the gas accumulator. Bernoulli's equation now becomes

$$F_p = \frac{\rho A_p^3}{2k^2 A(x)^2} v_p^2 + c v_p + f_{gas} \qquad (5)$$

For the presented damper, the diameter of the piston rod is only 12.7cm. This diameter value makes the area difference between the magnet chamber side and fluid volume side of a piston head is less than 8%. Therefore, we can assume the accumulator force $f_{gas} \cong 0$. Also, scatter plots show that friction is negligible for most gap sizes and a quadratic representation is more than adequate to model the data. This implies that $c \cong 0$. Friction details will be discussed further in the results portion of the thesis.

We now turn our attention to the main focus of this chapter: the effective orifice area function, $A(x)$. A hypothesis for $A(x)$ is developed by modifying equation (1) to incorporate a function of the gap size, x. We assume that the fluid "sees" the orifice as a virtual cylinder. The cylinder has a radius of $\frac{o_d}{2}$ and a height of x. Therefore, the cylinder area $A_{in} = 2\pi(\frac{o_d}{2} * x)$. As the gap widens, the cylinder surface area increases linearly until the limiting $A_{\max}$ function is reached and increases in gap no longer allow for greater fluid flow. Now, we have an hypothesis function

$$\hat{A}(x) = \min\{A_{in}(x), A_{\max}\} \qquad (6)$$

It is important to notice that $\hat{A}(x) \to A_{\max}$ as $x \to \infty$. This implies that once the gap becomes significantly larger than the orifice diameter, the magnet is no longer acting as a

valve and the orifice is the sole limiter to the flow of the fluid. The next section will present an experiment and data results to justify the above hypothesis.

CHAPTER FOUR

Experiment Results and Conclusions

In this chapter, we want to experimentally examine the effective orifice area, $A(x)$, and the force-velocity characteristics of the damper as a function of the applied current, $F(I)$. Separate experiments were conducted for each query and presented within the chapter. The presented results are for two separate damper designs. Initially, a damper was constructed with a cylinder wall of a clear plastic for viewing purposes. This damper, referred to as the "clear" damper, was previously presented by Levins and Gravagne [12]. Upon reviewing the results of the clear damper, a new damper was constructed with a high tolerance steel cylinder wall in order to relieve noisy data in the system. This cylinder is referred to as the "steel" cylinder. The gap experiment data for each cylinder is presented initially, followed by the applied current experimentation results.

Effective Orifice Area Experiments

Effective Orifice Area Experiment of Clear Cylinder

Testing for the clear cylinder was conducted on an exercise machine. The stroke data was recorded using a 500 lb. tension/compression load cell (Transducer Technologies SSM-500 with calibrated signal conditioner) and an externally mounted digital position sensor (Unimeasure LX-EP-15) for the force and linear displacement/velocity measurements, respectively. Figure 5 shows the testing set-up of the clear cylinder.

For this experiment, the piston head contained 3 orifices of 2.68mm in diameter. Therefore, A_{max} consists of 3 inlet areas in "parallel" with each other, and in series with the outlet check valve orifice,

$$A_{in} = 3\pi\left(\frac{2.68}{2}\right)^2; \quad A_{out} = \pi\left(\frac{3.22}{2}\right)^2$$

$$A_{\max} = \frac{A_{in}A_{out}}{A_{in} + A_{out}} = 5.49\,\text{mm}^2 \tag{7}$$

Thus, the hypothesis of $A(x)$ modifies equation (7) by assuming the total cylinder surface area is $3\times(2\pi\times 1.34x) \cong 8\pi x$. Therefore, the hypothesis function

$$\hat{A}(x) = \frac{\min\{8\pi x, A_{in}\}\times A_{out}}{\min\{8\pi x, A_{in}\} + A_{out}} \tag{8}$$

Clear Cylinder Effective Orifice Area Experiment Results

The gap, x, was fixed at 5 different positions,

$$x \in \{0.25,0.51,0.76,1.02,1.14\} \text{ millimeters} \tag{9}$$

For each gap size, force-velocity data was gathered and plotted with a least square error best fit curve. Figure 6 shows a sample of the scatter plot data and best fit curve for the gap experiment. The quadratic stiffness coefficients for the cylinder gap experiment were found to be

$$Q(x) = \frac{\rho A_p^2}{2k^2 A(x)^2} \in \{195,136,116,117,116\}\times 10^3 \tag{10}$$

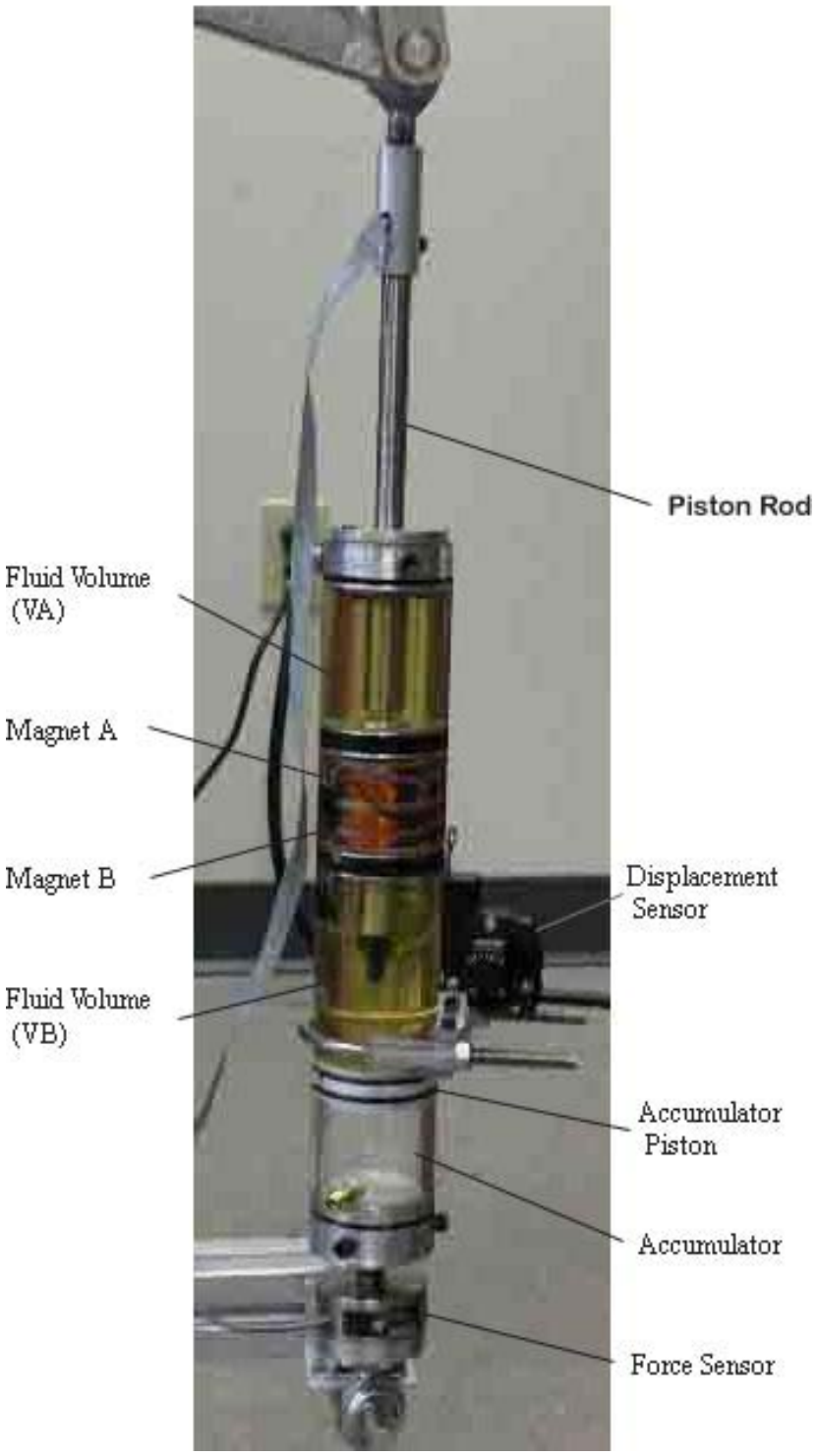

Figure 5: Testing Set-Up for Clear Cylinder – View of the clear cylinder mounted on the testing machine.

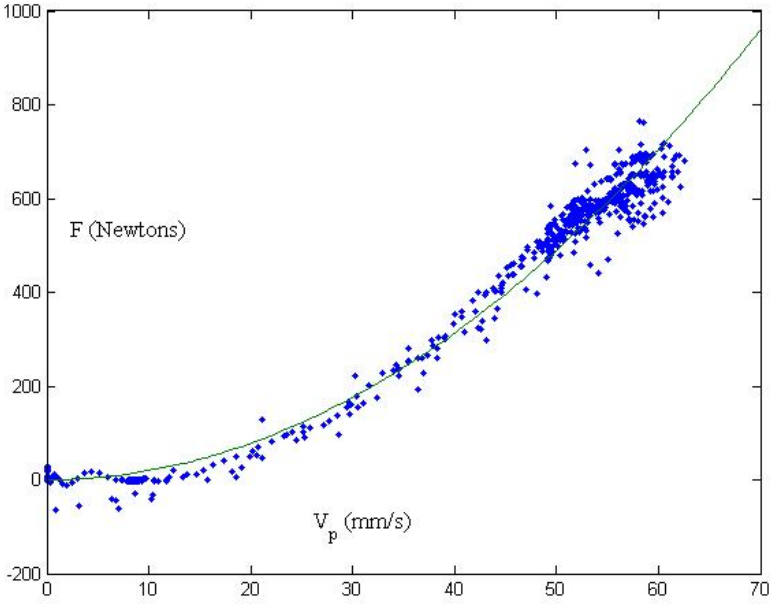

Figure 6: Sample Force-Velocity Data for 0.25mm Gap – Scatter plot data for the compression stroke of the clear cylinder with a 0.25mm gap.

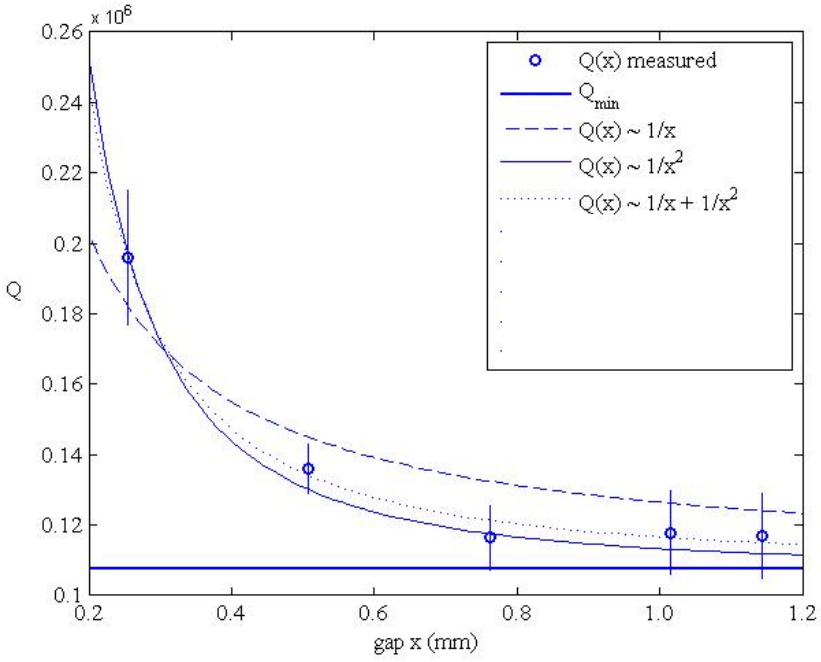

Figure 7: Q Versus Gap Size for Clear Cylinder – plot of $Q(x)$ showing measured values and least square best fit curves. Vertical error bars indicate one standard deviation.

This data suggests that $Q(x)$ approaches a minimum value, Q_{min}. This is easily predicted if we recall that $A(x) \to A_{\max}$ as $x \to \infty$. The piston head for this design had a diameter of 47.5mm, and the hydraulic fluid used in the experiment had a mass density of approximately 900 kg/m^3. Using k = 0.9, it was found that $Q_{min} = 107.2 * 10^3$. $Q(x)$ is plotted in figure 7 along with several different modeling functions. The modeling function of $\frac{1}{x^2}$ showed to fit the data accurately and resulted in a $Q(x) = \frac{0.0058}{x^2} + Q_{\min}$ best fit curve.

Rearranging equation (10) for the valved orifice area function, $A(x)$, gives

$$A(x) = \sqrt{\frac{\rho A_p^3}{2k^2} \frac{x^2}{Q_{\min} x^2 + 0.0058}} \qquad (11)$$

The effective valved orifice area is plotted in figure 8 against the hypothesis function. The plot showed that the hypothesis function is fairly accurate in its prediction. Due to accuracy of the hypothetical applied orifice function to the experimental data of the clear cylinder, the same hypothesis was utilized to analyze the steel cylinder.

Finally, figure 7 illustrates the fact that only a small gap is needed between the magnets to achieve an efficient valve. The effective orifice area increases over 90% within the first 0.5mm of movement by the magnetic valve. Note that this is highly important due to the fact that magnetic field strength increases the closer the magnets are in proximity.

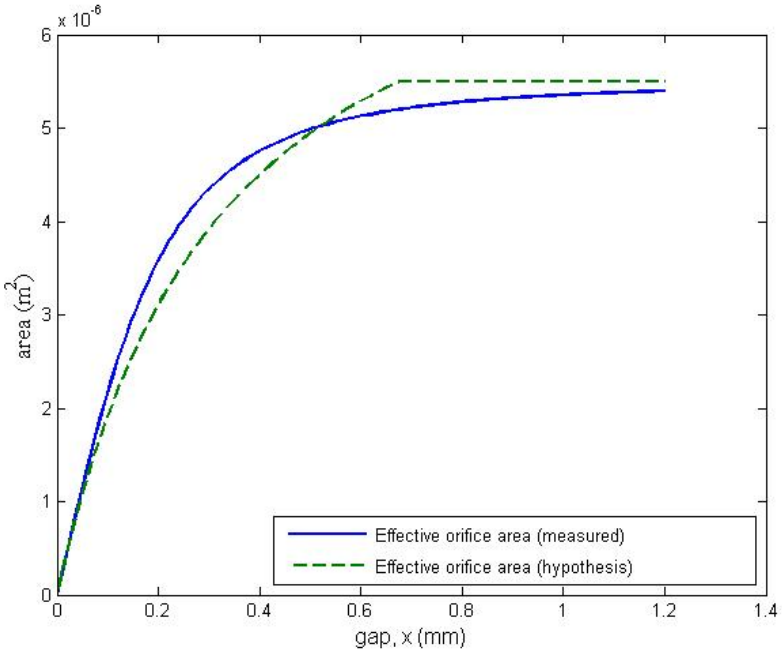

Figure 8: Clear Cylinder Effective Orifice Area – comparison of the measured effective orifice area function and the hypothesis function.

Effective Orifice Area Experiment of Testing Piston

In order to further demonstrate the variable orifice phenomenon, a simpler, separate piston was designed and tested to allow for more variability in gap size. The piston, shown below in figure 9, consists of a piston head with a single orifice and a fluid blocking surface. The blocking surface is threaded and attached to the piston head by a bolt. This design allowed for testing of a wider range of gap distances. The piston was tested using the lever assembly shown in figure 10 and used the same previously described force and displacement/velocity sensors. Figure 11 shows a close-up of the damper body when it is in the lever assembly.

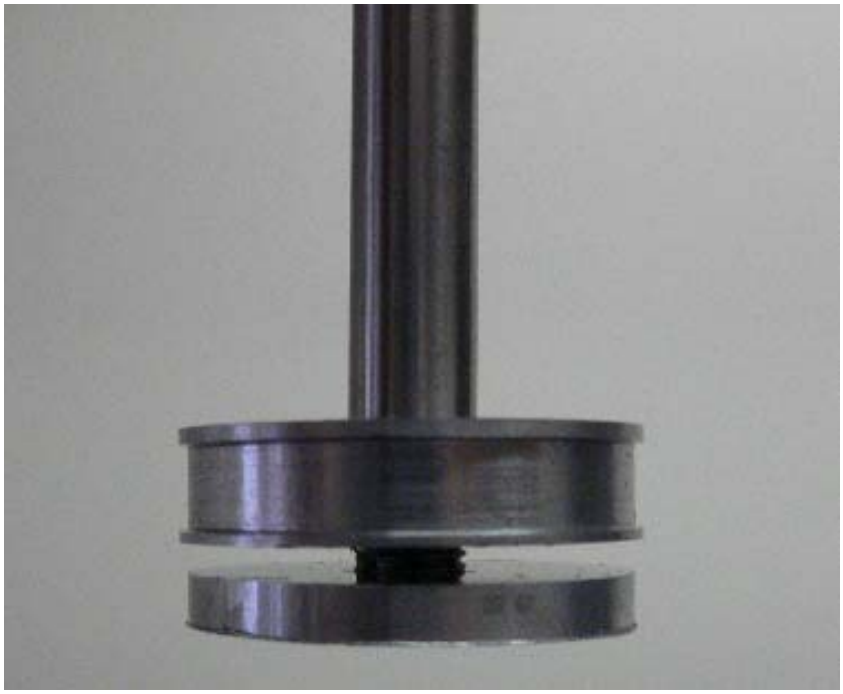

Figure 9: Piston Head for Gap Testing – The piston head assembly for the gap testing. The assembly consists of a piston head with a single orifice and a fluid blocking surface. The fluid blocking surface is threaded and connected with a bolt, allowing for the gap size to be easily adjusted.

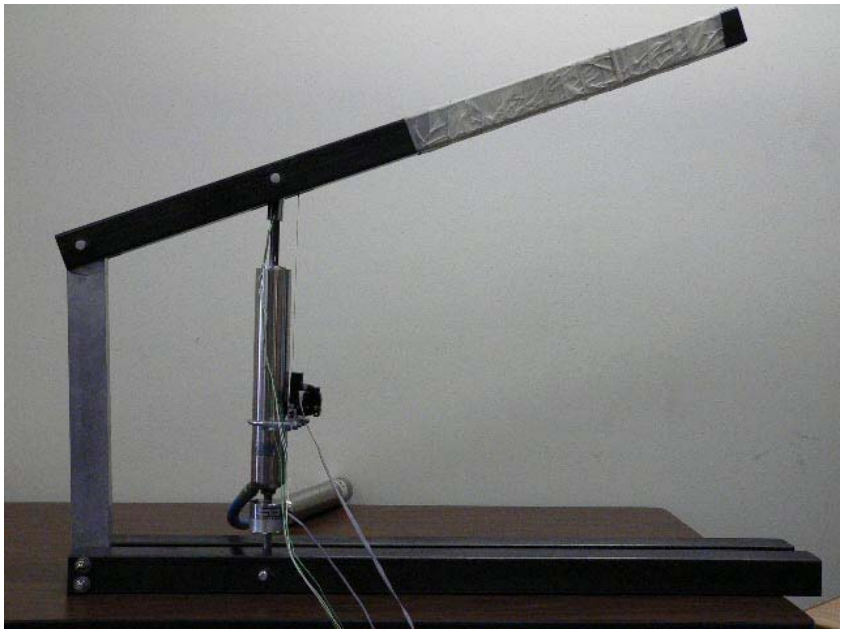

Figure 10: Testing Lever Assembly – The lever assembly used for gathering test data. The lever assembly consists of a fixed base, post, and lever. Two plastic bearings connect the post and lever allowing for low friction, vertical movement of the lever. The piston connects to the base and lever when testing.

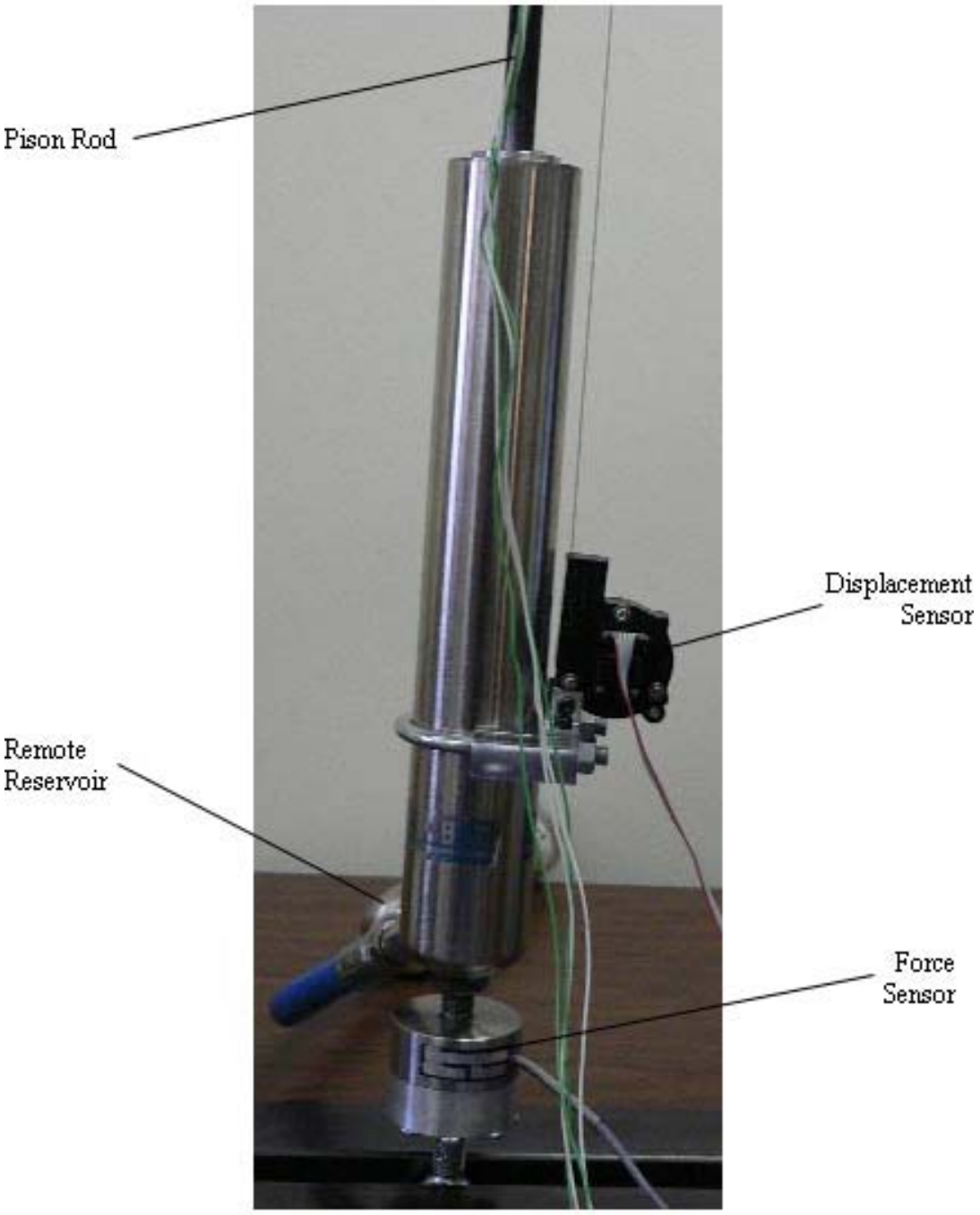

Figure 11: Close-up of Piston when Mounted on Lever Assembly – The damper when mounted on the lever assembly with the force and displacement sensors used to collect the testing data.

Testing Piston Effective Orifice Area Experiment Results

The experimental piston was tested at 6 different gap distances,

$$x \in \{0.27, 0.36, 0.45, 0.60, 0.84, 1.2\} \text{ millimeters} \quad (12)$$

The experimental piston head has only one orifice with a diameter of 2.49mm instead of three orifices like the piston head of the clear cylinder. This leaves A_{max} to be calculated as,

$$A_{\max} = \pi\left(\frac{2.49}{2}\right)^2 = 4.87mm^2 \quad (13)$$

This diameter size also presents the hypothesis cylinder area from equation (6) to be $A_{in} = 2\pi(1.25 * x) \cong 2.5\pi x \text{ mm}^2$. For each of the gap distances, force-velocity scatter plots were obtained through the experimental setup previously described, and least square error best-fit curves were determined to give quadratic stiffness coefficients for equation 5 as

$$Q(x) = \frac{\rho A_p^2}{2k^2 A(x)^2} \in \{145, 123, 105, 100, 97.5, 97.2\} \times 10^3 \quad (14)$$

Force-velocity scatter plots for the gap sizes of 0.27mm and 1.2mm are shown in figures 12 and 13, respectively. The scatter data is plotted with the best fit curve corresponding to the gap size. It is important to be aware that a linear element was added to the best fit curve in the larger gap size in order to fit the data better. This linear element is due to the friction between the piston rod and the top seal of the damper as the rod is moving. This friction is not seen in the smaller gap size plot because the force required to displace the fluid through the smaller orifice is so much larger than the frictional force that the fluid force overshadows the frictional force. Without the

frictional force, the cylinder behaves in the quadratic nature one would expect. The damper was only tested for larger gap sizes in order to see if the effective orifice area would, in fact, approach A_{max}. Therefore, since the friction was not prevalent in the gap data that was most crucial to the modeling of the damper, the velocity dependant friction in equation 5 was able to be disregarded.

Also notice in figure 12, the scatter plot of the smaller gap size, that a constant force offset needed to be added to fit the data. Since the smaller gap size represents a smaller orifice, the magnetic valve is able to resist a larger static pressure before displacing from the piston head and allowing the piston to move.

Some ambient data points can be seen in figure 12 as well. These data points can be attributed to pressures in the remote reservoir. The points represent a stroke of the damper but do not correspond to the actual characteristics of the damper. The remote reservoir of the shock was filled with 120 psi of air. When the differential pressure across the piston heads during a stroke exceeded the reservoir pressure, the air within the reservoir was compressed. The compression of the air in the remote reservoir of the damper caused the piston to spring back and create the “trampoline points” seen in the plot. The pressure in the reservoir prompted the piston to move at a high velocity with a low force, as shown by the trampoline points in the plot. The reservoir continued to push the piston until enough fluid passed through the orifice to allow the pressure in the reservoir to once again exceed the differential pressure on the piston heads. At this point, the data points once again tracked the true characteristics of the damper. In order to minimize the amount of trampoline points in the scatter plot data, the damper was held

after a compression stroke until the pressure in the reservoir was once again larger than the differential pressure of the fluid volumes.

Plots of each of the Q values against the gap distance, as well as the least square best-fit line for $Q(x)$, are shown in figure 14. The plot also indicates that $Q(x)$ asymptotically approaches a lower bound, Q_{min}, much like the $Q(x)$ for the clear cylinder. The experimental piston head is 45.72mm in diameter, and, using a graduated cylinder and digital scale, the density of the fluid was calculated to be 843 kg/m^3. By allowing k = 0.9, it was determined that $Q_{min} = 97.23 \times 10^3$. This value of Q_{min} agrees well with the asymptotic approach of the modeling equation for $Q(x)$.

Figure 14 also contains the hypothesis function of $Q(x)$. Notice how the hypothesis function increases much more rapidly than the measured function. This can be attributed to a number of factors. First, if the piston head does not fully seal with the inside of the damper body, fluid will escape around the outside of the piston head instead of flowing solely through the orifice. This effect will cause the Q values to flatten out much like on the figure. This makes sense, intuitively, because the extra fluid escaping would represent a larger orifice size. In turn, a larger orifice size would represent a smaller Q value.

Secondly, due to the rod sliding past the top seal, a small amount of velocity dependent friction is implemented into the system. This small amount of friction would introduce a linear component into the modeling equation that would also aid in flattening out the data. Any combination of these two factors could contribute to the slight discrepancy between the hypothetical behavior and the actual behavior of the damper.

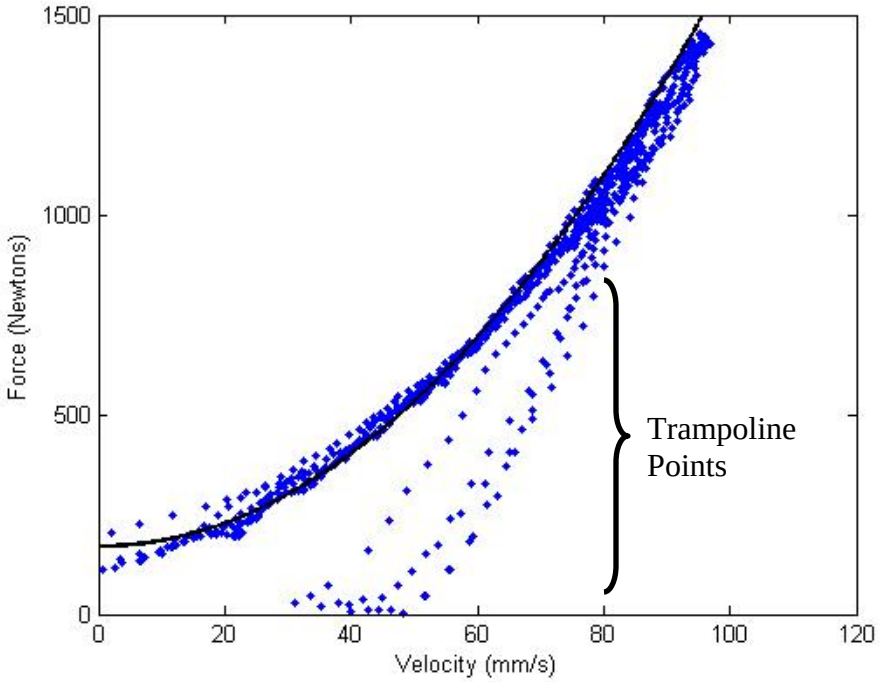

Figure 12: Force-Velocity Data for 0.27mm Gap – Scatter plot data and corresponding least square best fit curve for 0.27mm gap testing.

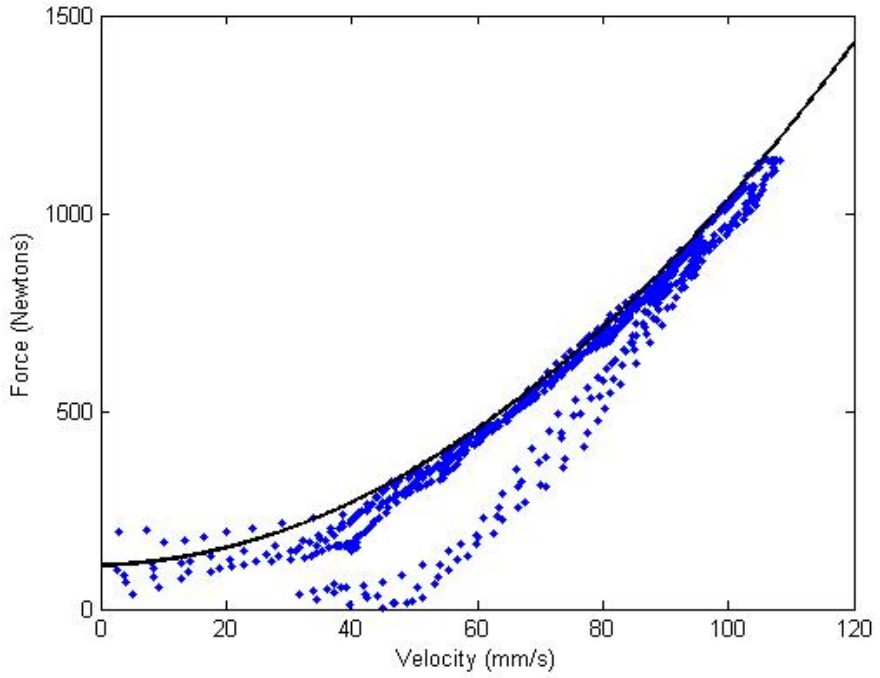

Figure 13: Force-Velocity Data for 1.20mm Gap – Scatter plot data and corresponding least square best fit curve for 1.20mm gap testing.

The important aspect to take from figure 14 is the fact that the experimental data does follow the relationship we expect. The *Q* values exponentially decrease with larger gap sizes and begin to approach the Q_{min} value that represents the maximum orifice area, A_{max}.

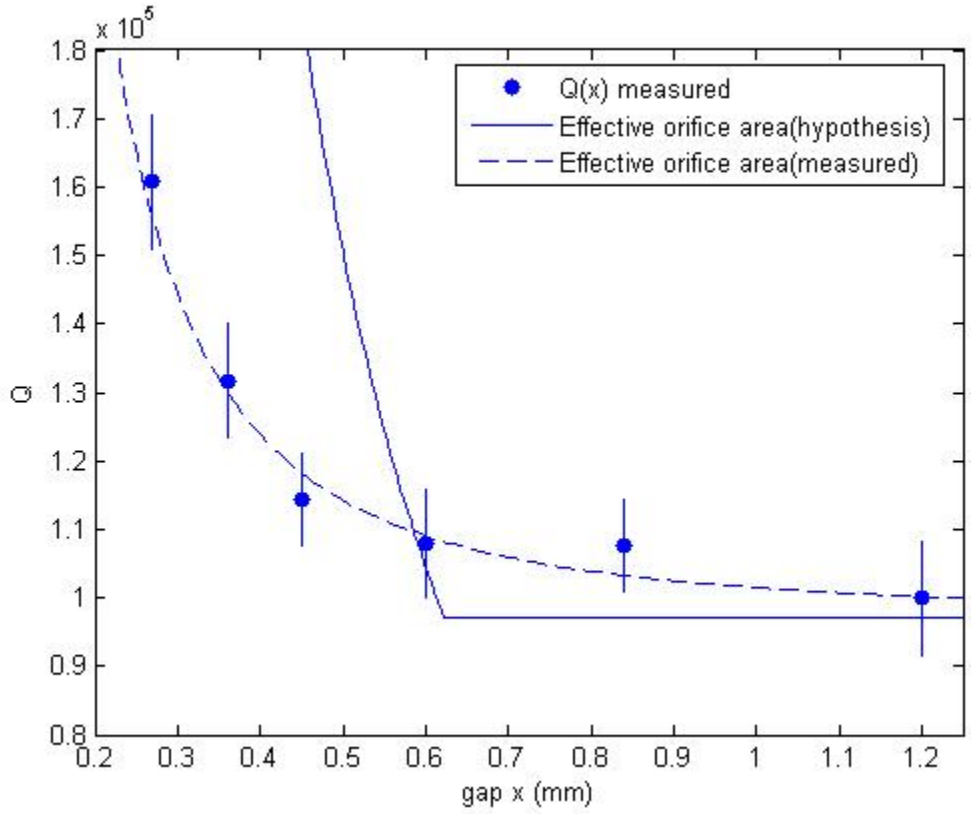

Figure 14: Q Versus Gap Size for Steel Cylinder – Comparison of the calculated *Q* values and corresponding least square best fit curve to the hypothetical *Q*(*x*) function presented in the chapter. Vertical error bars indicate one standard deviation.

Magnetic Strength Experiments

Description of Magnetic Strength Experiment

In the previous experiment, the gap size in between the magnets was constrained in order to explore the activity of the magnetic valve. In this experiment, we allow the magnets to freely move and vary the current applied to each of the magnets. As

mentioned before, the amount of applied current controls the strength of the magnetic field, which, in turn, controls the regulation of the gap size for the magnetic valve. Also as in the gap experiment, an exercise machine was used to collect force-velocity data for the clear cylinder and the lever assembly was used to collect the force-velocity data for the steel cylinder.

Clear Cylinder Magnetic Strength Experiment Results

Force-velocity data was recorded for 8 different current values,

$$I \in \{0,380,770,1150,1540,1930,2260,2600\} \text{ milliamps} \quad (15)$$

Figure 15 shows the second-order best fit polynomials of the compression and extension strokes for the 8 different current values. The scatter plot data was omitted for readability. For this damper, the resistance increases 107% at a speed of 50 mm/s when 2.6A of current is applied. Notice that there is no constant offset for the polynomials on this plot. This behavior is unexpected and insinuates that the damper is acting more like the model of the theoretical damper instead of exhibiting common difficultly-predicted characteristics of dampers.

Steel Cylinder Magnetic Strength Experiment Results

Force-velocity data for the damper was gathered for a series of applied currents,

$$I \in \{0,260,521,781,1042,1302,1563,1823,2083\} \text{ milliamps} \quad (16)$$

For each set of force-velocity data, a second order least-square best fit function was conformed to the raw data. Figure 16 is an example of the raw force-velocity data with its corresponding best fit curve. The previously described trampoline points are also present in the magnetic strength experiment results of the steel cylinder.

Although the trampoline points are present in the steel cylinder data, the true characteristics of the cylinder are easily visible. The discernible cylinder characteristics allow the trampoline points to be ignored. Also, for plots of the lower current values, $I \in \{0,260,521,781\}$, a linear variable needed to be added to the modeling equation for the best fit curve, much like the larger gap sizes of the gap experiment. This linear variable can be attributed to the velocity dependent friction from the piston rod and seals within the cylinder. It is not visible in the larger currents primarily because the larger forces from the magnetic valve begin to "drown out" the friction forces. Figure 17 shows the best fit curves for each of the applied currents for both the compression and extension strokes. The scatter plot data has been eliminated from this plot for readability. This plot shows that at a speed of 40 mm/s, the resistance of the damper increases by 161% when a current of 2.083 A is applied to the magnets.

This increase in resistance is quite evident to the user due to the fact that at this applied current, the resistance severely dampens the cylinder, almost to the point of "locking up" the cylinder. Also notice how the constant offsets on each the best fit curves increase as the current increases. This increase in the constant offset is expected since as the magnetic field strength increases, a stronger static pressure must initially build up to displace the magnet from the piston head and allow fluid to flow through the orifice. These offsets correlate with the constant offsets that needed to be added to the smaller gap data for the gap experiment. Finally, the groupings of the best fit curves at low currents and high currents fall exactly how one would expect functions of magnetic fields to plot. When dealing with electromagnets, the strength of the magnetic field will often rise in an exponential fashion.

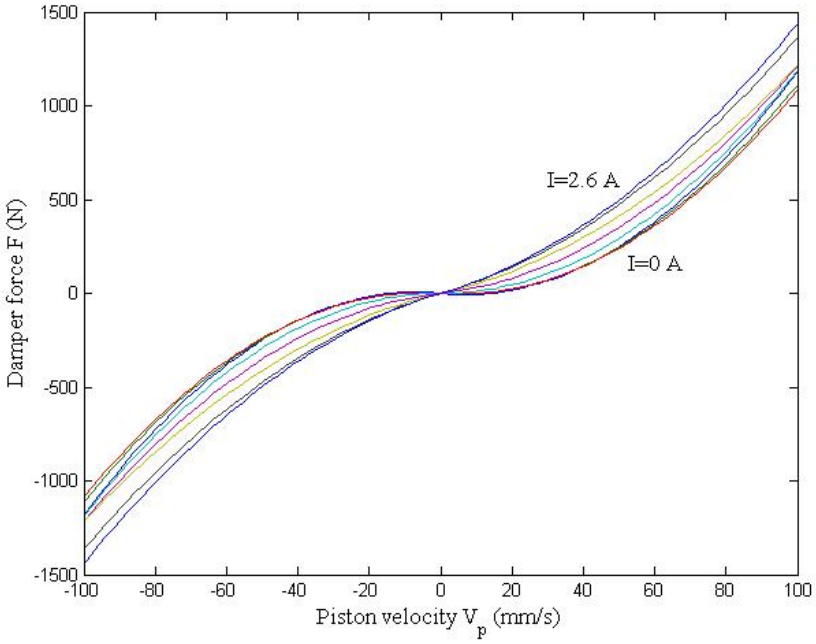

Figure 15: Force-Velocity Characteristics from Applied Current for Clear Cylinder - Least square best fit curves for the extension and compression strokes of the clear damper for each applied current.

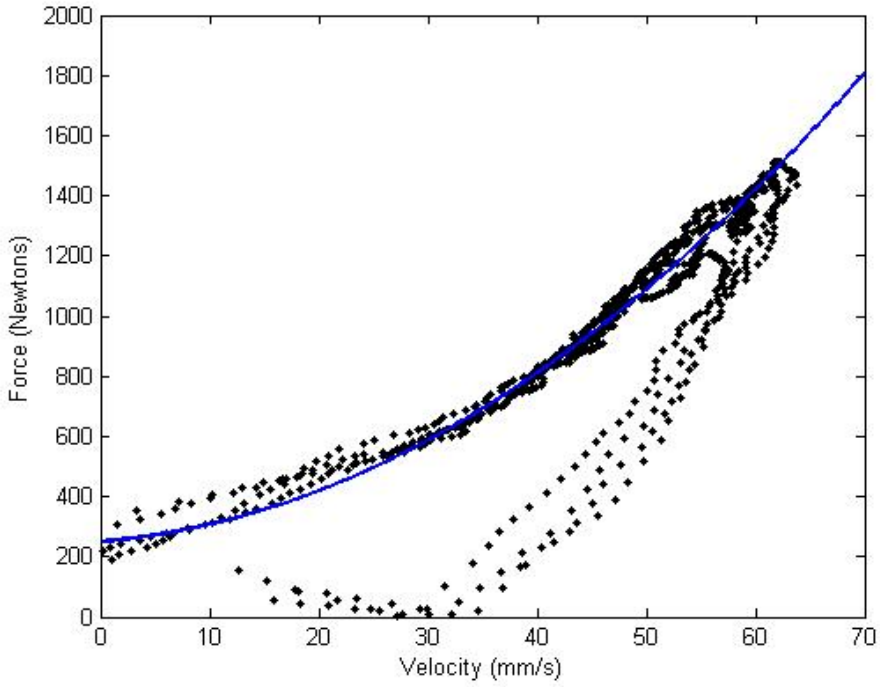

Figure 16: Sample Force-Velocity data for the Magnetic Strength Experiment - Force-velocity data for I = 260mA and the corresponding least square best fit curve.

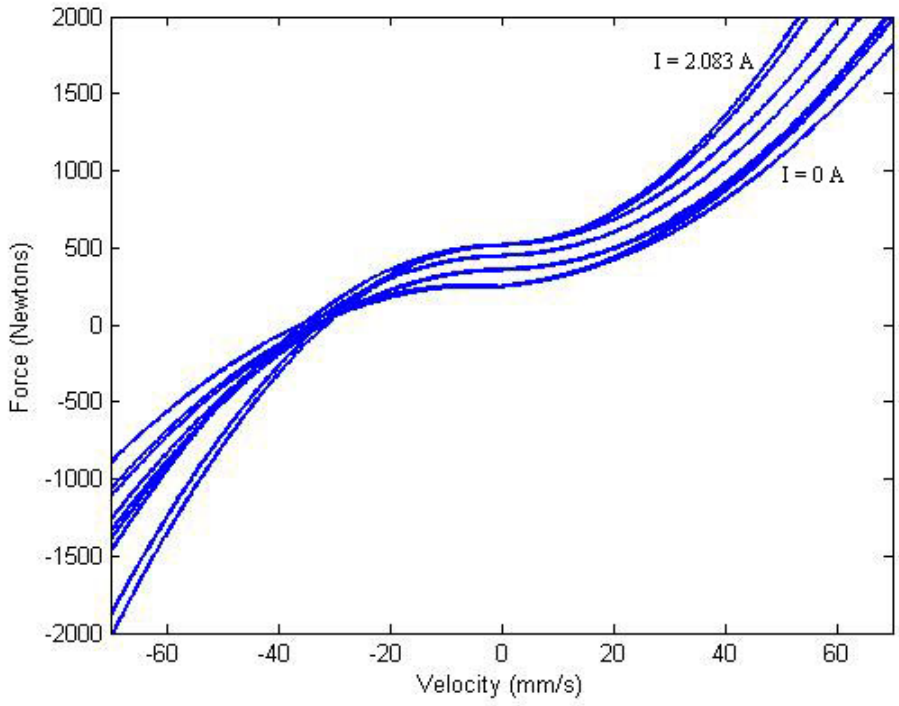

Figure 17: Force-Velocity Characteristics from Applied Current for Steel Cylinder - Least square best fit curves for the extension and compression strokes of the steel damper for each applied current.

Conversely, as the magnets begin to reach the maximum magnetic field they are able to produce, often referred to as saturation, the magnetic field strength begins to decrease in an exponential fashion. This activity is seen in this plot.

Comparison of Steel Cylinder and Clear Cylinder Data

The hypothesis function, $A(x)$, showed to followed the data for the clear cylinder relatively well; even though 3 of the $Q(x)$ values fell close to the value of Q_{min}. Therefore, the piston head was redesigned for the steel cylinder with a smaller orifice in order to test in a larger force range. The author hoped the larger force range would

produce more definitive values of $Q(x)$ for the new cylinder. Also, more testing was conducted with gap sizes that fell on the quadratic curve, $Q(x)$, of the clear cylinder. The hypothesis function of the gap testing cylinder did not follow the $Q(x)$ data of the gap testing piston as well as the hypothesis function of the clear cylinder followed its respective data. Several suggestions were mentioned regarding the behavior of the gap testing cylinder. In redesigning the damper for the steel cylinder, it was desirable to increase the range of the damper resistance due to the applied current. Therefore, the length of the electromagnets was slightly increased and a larger gauge of wire was used for the winding. The larger gauge wire lowered the winding resistance to allow for more current. Increasing current would, in turn, increase the strength of the magnetic field force. Upon testing, the larger magnets significantly increased the resistance range of the steel cylinder from that of the clear cylinder.

Even though the hypothesis effective orifice area for the testing piston did not follow values of $Q(x)$ as well as the hypothesis function for the clear damper, the implementation and examination of the testing piston proved that the hypothesis has some validity. Also, the redesign of the magnets helped to significantly increase the resistance of the steel damper over the clear damper. This increase in resistance makes the steel cylinder more usable in an exercising situation.

Conclusions

This thesis presents a design for an adjustable damper that can be implemented into exercise equipment. The design satisfies the design requirements of simplicity and internal, dynamic resistance control. After examining current adjustable damper and

fluid technologies, it was decided that dampers in exercise equipment would benefit the most from an adjustable orifice design.

Using two oppositely poled electromagnets, a magnetic valve has been designed and described. Analysis of the magnetic valve showed a significant correlation between the size of the gap separating the magnet and piston head, and the effective size of the orifices on the piston head. The hypothesis function of the magnetic valve matched reasonably well with the presented force-velocity of the two different dampers. The hypothesis function of the clear damper correlated with its respective data the better than the hypothesis function of the steel damper.

Finally, the force-velocity characteristics for a range of applied currents were also analyzed to demonstrate the strength characteristics of the two developed dampers. The characteristics of the clear damper closely followed the theoretical expectation, where the steel damper acted as expected. In addition, the testing and analysis showed that the steel damper provided a wider range of resistance control depending on the applied current. At a maximum current value, the damper became quite difficult to move for exercisers.

If recent trends continue, fluid damper resistance for exercise equipment will become more and more prevalent. This thesis presents solutions for internal resistance adjustability, although future work is still needed. The relationship between the applied current and the gap size still need to be quantified in order to provide a damper that can be dynamically controlled using feedback.

The following appendices provide code used to collect and process the data for each experiment. Also, the scatter plots for each of the data sets in the experiments are provided with the corresponding least square error best fit curve.

APPENDICES

APPENDIX A

MATLAB Code – Gap data

Readin.m

```
%This function reads in data column values from Excel spreadsheets
%and loads them into corresponding vectors

force_018raw=dlmread('018forcedata.xls','\t');
vel_018raw=dlmread('018veldata.xls','\t');
press_018raw=dlmread('018pressdata.xls','\t');
force_027raw=dlmread('027forcedata.xls','\t');
vel_027raw=dlmread('027veldata.xls','\t');
press_027raw=dlmread('027pressdata.xls','\t');
force_036raw=dlmread('036forcedata.xls','\t');
vel_036raw=dlmread('036veldata.xls','\t');
press_036raw=dlmread('036pressdata.xls','\t');
force_045raw=dlmread('045forcedata.xls','\t');
vel_045raw=dlmread('045veldata.xls','\t');
press_045raw=dlmread('045pressdata.xls','\t');
force_060raw=dlmread('060forcedata.xls','\t');
vel_060raw=dlmread('060veldata.xls','\t');
press_060raw=dlmread('060pressdata.xls','\t');
force_084raw=dlmread('084forcedata.xls','\t');
vel_084raw=dlmread('084veldata.xls','\t');
press_084raw=dlmread('084pressdata.xls','\t');
force_120raw=dlmread('120forcedata.xls','\t');
vel_120raw=dlmread('120veldata.xls','\t');
press_120raw=dlmread('120pressdata.xls','\t');
```

process.m

```
%This function calls the function 'convert' and places the returned vectors
%into corresponding vector names


[force_018, vel_018] = convert(force_018raw, vel_018raw);
[force_027, vel_027] = convert(force_027raw, vel_027raw);
[force_036, vel_036] = convert(force_036raw, vel_036raw);
[force_045, vel_045] = convert(force_045raw, vel_045raw);
[force_060, vel_060] = convert(force_060raw, vel_060raw);
[force_084, vel_084] = convert(force_084raw, vel_084raw);
[force_120, vel_120] = convert(force_120raw, vel_120raw);
```

convert.m

```
%This function takes the passed in force and velocity vectors and crops
%them to the same size.  It also converts the vectors into metric units
%before returning them


function [force_out,vel_out] = convert(force_in,vel_in)

   forcelength = length(force_in);
   vellength = length(vel_in);

   if(vellength>forcelength)                    %compare to see which vector is longer
      vel_out(:,2) = vel_in(1:forcelength,2);       %cropping longer vector
      force_out = force_in;
   end

   if(forcelength>vellength)
      force_out(:,2) = force_in(1:vellength,2);
      vel_out = vel_in;
   end

   vel_out(:,2) = 0.0254*vel_out(:,2);              %converting to meters
   force_out(:,2) = 4.44822162*100*force_out(:,2);     %converting to Newtons
```

get_ext_stroke.m

```
%This function calls the function 'ext_stroke' for each of the data sets


[force_018_ext, vel_018_ext] = ext_stroke(force_018,vel_018);
[force_027_ext, vel_027_ext] = ext_stroke(force_027,vel_027);
[force_036_ext, vel_036_ext] = ext_stroke(force_036,vel_036);
[force_045_ext, vel_045_ext] = ext_stroke(force_045,vel_045);
[force_060_ext, vel_060_ext] = ext_stroke(force_060,vel_060);
[force_084_ext, vel_084_ext] = ext_stroke(force_084,vel_084);
[force_120_ext, vel_120_ext] = ext_stroke(force_120,vel_120);
```

ext_stroke.m

```
%This function reads in complete force and velocity vectors and finds the
%data points corresponding to the extension stroke (positive force and velocity
%together).  A new vector is created with these data points and returned.


function [force_out, vel_out] = ext_stroke(force_in, vel_in)

index = 6;                          %index for syncronizing force and velocity data

ind = find(force_in(:,2) > 0);          %find indices of positive force

for i=1:length(ind),                    %build vectors for positive indices
   force_out(i) = force_in(ind(i),2);
   if((ind(i) + index) > length(vel_in))
      vel_out(i) = vel_in(ind(i),2);
   else
      vel_out(i) = vel_in(ind(i) + index,2);
   end
end
```

avals.m

```
%This function calls function 'geta' and uses the returned values to plot
%against the gap distances


a1 = geta(force_018_ext,vel_018_ext);   %function call to obtain a values
mean_a1 = mean(medfilt1(a1,500))        %filters the data to remove ambient data
a2 = geta(force_027_ext,vel_027_ext);
mean_a2 = mean(medfilt1(a2,500))
a3 = geta(force_036_ext,vel_036_ext);
mean_a3 = mean(medfilt1(a3,500))
a4 = geta(force_045_ext,vel_045_ext);
mean_a4 = mean(medfilt1(a4,500))
a5 = geta(force_060_ext,vel_060_ext);
mean_a5 = mean(medfilt1(a5,500))
a6 = geta(force_084_ext,vel_084_ext);
mean_a6 = mean(medfilt1(a6,500))
a7 = geta(force_120_ext,vel_120_ext);
mean_a7 = mean(medfilt1(a7,500))


mean_a = [mean_a2 mean_a3 mean_a4 mean_a5 mean_a6 mean_a7];
x = [0.27 0.36 0.45 0.60 0.84 1.2];

plot(x, mean_a,'.','markersize',20)     %plots the averaged a values against the gap
distances
%axis([0.2 1.4 0.09 0.18]);
```

geta.m

```
%This function calculates and returns the a value for each of the data
%points within the force and velocity data sets.


function a = geta(force_in,vel_in)

   for i=1:length(vel_in)
      a(i) = force_in(i)/(vel_in(i)*vel_in(i));   %calculate a from equation f = a*v^2
   end
```

Qvals.m

```
%This function calculates Bernoulli's equation for the given orifice size
%and calculates the modeling line.  vec_in is a vector containing the
%mean_a values for the data sets.  This function then plots the Bernoulli
%line on the same plot as the a versus gap size values.


function Qvals(mean_a,s)

x = [0.27 0.36 0.45 0.60 0.84 1.2];        %vector of gap sizes
orifice = 2.4892;                          %orifice diameter in mm

k = 0.9;                                   %constant in Bernoulli's eq.
p = 843;                                   %density of the fluid
Ap = pi*(45.72/2000)^2;                    %area of the piston head
Ain = pi*(orifice/2000)^2;                 %area of the orifice

tempx = linspace(.23,1.25,250);
for i=1:length(tempx)
   temp = 2*pi*(orifice/2000)*(tempx(i)/1000);     %calculation of input area
   if (temp < Ain)                         %comparison between calculated input area and
maximum input area
      Q(i) = (p*Ap^3)/(2*k^2*temp^2);          %calculation of Bernoulli's equation
   else
      Q(i) = (p*Ap^3)/(2*k^2*Ain^2);
   end
end
Q(240)

plot(x,mean_a,'.','markersize',20);        %plot of a values versus gap sizes
hold on
axis([0.2 1.25 0.8*10^5 1.8*10^5]);
plot(tempx, Q)                             %plot of Bernoulli's equation
xlabel('gap x (mm)');
ylabel('Q');

x2 = linspace(0,2,250);
hold on
plot(x2,4250./(x2.*x2)+97230,'--');
line([.27 .27], [(mean_a(1) - s(2)) (mean_a(1) + s(2))]);      %plot vertical deviation line
line([.36 .36], [(mean_a(2) - s(3)) (mean_a(2) + s(3))]);
```

```
line([.45 .45], [(mean_a(3) - s(4)) (mean_a(3) + s(4))]);
line([.60 .60], [(mean_a(4) - s(5)) (mean_a(4) + s(5))]);
line([.84 .84], [(mean_a(5) - s(6)) (mean_a(5) + s(6))]);
line([1.20 1.20], [(mean_a(6) - s(7)) (mean_a(6) + s(7))]);
hold off

legend('Q(x) measured','Effective orifice area(hypothesis)','Effective orifice
area(measured)');
```

plotFV.m

```
%This function plots the force/velocity characteristics for each of the
%different gap size data sets.  The plots are in subplot format.


index = 5;                  %value used to syncronize data

subplot(2,2,1);
plot(vel_027(3+index:length(vel_027),2),force_027(3:length(vel_027)-index,2),'.');
%plot raw data
hold on
plot(x,.15*x.^2+0.14*x+0.5, 'k', 'linewidth', 2)       %plot best-fit line
hold off
title('0.25mm gap');
axis([0 4 0 2]);

subplot(2,2,2);
plot(vel_036(3+index:length(vel_036),2),force_036(3:length(vel_036)-index,2),'.');
hold on
plot(x,.13*x.^2+0.11*x+0.5, 'k', 'linewidth', 2)
hold off
title('0.37mm gap');
axis([0 4 0 2]);

subplot(2,2,3);
plot(vel_045(3+index:length(vel_045),2),force_045(3:length(vel_045)-index,2),'.');
hold on
plot(x,.11*x.^2+0.10*x+0.5, 'k', 'linewidth', 2)
hold off
title('0.51mm gap');
axis([0 4 0 2]);

index = 5;

subplot(2,2,4);
plot(vel_060(3+index:length(vel_060),2),force_060(3:length(vel_060)-index,2),'.');
hold on
plot(x,.095*x.^2+0.10*x+0.5, 'k', 'linewidth', 2)
hold off
title('0.66mm gap');
```

```
axis([0 4 0 2]);

figure(2)
subplot(2,2,1);
plot(vel_084(3+index:length(vel_084),2),force_084(3:length(vel_084)-index,2),'.');
hold on
plot(x,.0875*x.^2+0.10*x+0.5, 'k', 'linewidth', 2)
hold off
title('0.84mm gap');
axis([0 4 0 2]);

subplot(2,2,2);
plot(vel_120(3+index:length(vel_120),2),force_120(3:length(vel_120)-index,2),'.');
hold on
plot(x,.11*x.^2+0.10*x+0.5, 'k', 'linewidth', 2)
hold off
title('1.02mm gap');
axis([0 4 0 2]);

subplot(2,2,4);
plot(x,.15*x.^2+0.14*x+0.5, 'r', 'linewidth', 2)
hold on
plot(x,.13*x.^2+0.11*x+0.5, 'g', 'linewidth', 2)
plot(x,.11*x.^2+0.10*x+0.5, 'b', 'linewidth', 2)
plot(x,.095*x.^2+0.10*x+0.5, 'y', 'linewidth',2)
plot(x,.0875*x.^2+0.10*x+0.5, 'm', 'linewidth',2)
plot(x,.12*x.^2+0.08*x+0.5, 'k', 'linewidth', 2)
hold off
```

plotall.m

```
%This function plots all of the force-velocity data for the gap experiment
%in scatter plot form with different colors representing different data
%sets


index = 6;
hold on;
axis([0 6 0 4]);
plot(vel_027(3+index:length(vel_027),2),force_027(3:length(vel_027)-
index,2),'.','markeredgecolor','k');
pause(1);
plot(vel_036(3+index:length(vel_036),2),force_036(3:length(vel_036)-
index,2),'.','markeredgecolor','r');
pause(1);
plot(vel_045(3+index:length(vel_045),2),force_045(3:length(vel_045)-
index,2),'.','markeredgecolor','g');
pause(1);
plot(vel_060(3+index:length(vel_060),2),force_060(3:length(vel_060)-
index,2),'.','markeredgecolor','y');
pause(1);
plot(vel_084(3+index:length(vel_084),2),force_084(3:length(vel_084)-
index,2),'.','markeredgecolor','m');
pause(1);
plot(vel_120(3+index:length(vel_120),2),force_120(3:length(vel_120)-
index,2),'.','markeredgecolor','b');
```

stdev.m

```
%This function takes the given a values for the gap experiment and finds
%the corresponding standard deviation.  A vertical line is then plotted on
%top of the points to represent the range of the standard deviation


tempa1 = medfilt1(a1,500);          %filter incoming data
s1 = std(tempa1);                   %compute standard deviation
tempa2 = medfilt1(a2,500);
s2 = std(tempa2);
tempa3 = medfilt1(a3,500);
s3 = std(tempa3);
tempa4 = medfilt1(a4,500);
s4 = std(tempa4);
tempa5 = medfilt1(a5,500);
s5 = std(tempa5);
tempa6 = medfilt1(a6,500);
s6 = std(tempa6);
tempa7 = medfilt1(a7,500);
s7 = std(tempa7);

sd = [s1 s2 s3 s4 s5 s6 s7]


x2 = linspace(0,2,250);
hold on
plot(x2,4250./(x2.*x2)+97230,'--');
line([.27 .27], [(mean_a2 - s2) (mean_a2 + s2)]);      %plot vertical deviation line
line([.36 .36], [(mean_a3 - s3) (mean_a3 + s3)]);
line([.45 .45], [(mean_a4 - s4) (mean_a4 + s4)]);
line([.60 .60], [(mean_a5 - s5) (mean_a5 + s5)]);
line([.84 .84], [(mean_a6 - s6) (mean_a6 + s6)]);
line([1.20 1.20], [(mean_a7 - s7) (mean_a7 + s7)]);
hold off
```

APPENDIX B

MATLAB Code – Force-velocity Data from Applied Current

readin.m

```
%This function reads in data column values from Excel spreadsheets for the
%applied current experiment and loads them into corresponding vectors


force_0000raw=dlmread('0000forcedata.xls','\t');
vel_0000raw=dlmread('0000veldata.xls','\t');
press_0000raw=dlmread('0000pressdata.xls','\t');
force_0260raw=dlmread('0260forcedata.xls','\t');
vel_0260raw=dlmread('0260veldata.xls','\t');
press_0260raw=dlmread('0260pressdata.xls','\t');
force_0521raw=dlmread('0521forcedata.xls','\t');
vel_0521raw=dlmread('0521veldata.xls','\t');
press_0521raw=dlmread('0521pressdata.xls','\t');
force_0781raw=dlmread('0781forcedata.xls','\t');
vel_0781raw=dlmread('0781veldata.xls','\t');
press_0781raw=dlmread('0781pressdata.xls','\t');
force_1042raw=dlmread('1042forcedata.xls','\t');
vel_1042raw=dlmread('1042veldata.xls','\t');
press_1042raw=dlmread('1042pressdata.xls','\t');
force_1302raw=dlmread('1302forcedata.xls','\t');
vel_1302raw=dlmread('1302veldata.xls','\t');
press_1302raw=dlmread('1302pressdata.xls','\t');
force_1563raw=dlmread('1563forcedata.xls','\t');
vel_1563raw=dlmread('1563veldata.xls','\t');
press_1563raw=dlmread('1563pressdata.xls','\t');
force_1823raw=dlmread('1823forcedata.xls','\t');
vel_1823raw=dlmread('1823veldata.xls','\t');
press_1823raw=dlmread('1823pressdata.xls','\t');
force_2083raw=dlmread('2083forcedata.xls','\t');
vel_2083raw=dlmread('2083veldata.xls','\t');
press_2083raw=dlmread('2083pressdata.xls','\t');
```

process.m

```
%This function calls the function 'convert' and places the returned vectors
%into corresponding vector names


[force_0000, vel_0000] = convert(force_0000raw, vel_0000raw);
[force_0260, vel_0260] = convert(force_0260raw, vel_0260raw);
[force_0521, vel_0521] = convert(force_0521raw, vel_0521raw);
[force_0781, vel_0781] = convert(force_0781raw, vel_0781raw);
[force_1042, vel_1042] = convert(force_1042raw, vel_1042raw);
[force_1302, vel_1302] = convert(force_1302raw, vel_1302raw);
[force_1563, vel_1563] = convert(force_1563raw, vel_1563raw);
[force_1823, vel_1823] = convert(force_1823raw, vel_1823raw);
[force_2083, vel_2083] = convert(force_2083raw, vel_2083raw);
```

convert.m

```
%This function takes the passed in force and velocity vectors and crops
%them to the same size.  It also converts the vectors into metric units
%before returning them


function [force_out,vel_out] = convert(force_in,vel_in)

   forcelength = length(force_in);
   vellength = length(vel_in);

   if(vellength>forcelength)                    %compare to see which vector is longer
      vel_out(:,2) = vel_in(1:forcelength,2);       %cropping longer vector
      force_out = force_in;
   end

   if(forcelength>vellength)
      force_out(:,2) = force_in(1:vellength,2);
      vel_out = vel_in;
   end

   %vel_out(:,2) = 0.0254*vel_out(:,2);             %converting to meters
   vel_out(:,2) = 25.4*vel_out(:,2);               %converting to millimeters
   force_out(:,2) = 4.44822162*100*force_out(:,2);     %converting to Newtons
```

get_ext_stroke.m

```
%This function calls the function 'ext_stroke' for each of the data sets


[force_0000_ext, vel_0000_ext] = ext_stroke(force_0000,vel_0000);
[force_0260_ext, vel_0260_ext] = ext_stroke(force_0260,vel_0260);
[force_0521_ext, vel_0521_ext] = ext_stroke(force_0521,vel_0521);
[force_0781_ext, vel_0781_ext] = ext_stroke(force_0781,vel_0781);
[force_1042_ext, vel_1042_ext] = ext_stroke(force_1042,vel_1042);
[force_1302_ext, vel_1302_ext] = ext_stroke(force_1302,vel_1302);
[force_1563_ext, vel_1563_ext] = ext_stroke(force_1563,vel_1563);
[force_1823_ext, vel_1823_ext] = ext_stroke(force_1823,vel_1823);
[force_2083_ext, vel_2083_ext] = ext_stroke(force_2083,vel_2083);
```

ext_stroke.m

```
%This function reads in complete force and velocity vectors from the
%applied current experiments and finds the data points corresponding to the
%extension stroke (positive force and velocity together).  A new vector is
%created with these data points and returned.


function [force_out, vel_out] = ext_stroke(force_in, vel_in)

index = 6;                          %index for syncronizing force and velocity data

ind = find(force_in(:,2) > 0);          %find indices of positive force

for i=1:length(ind),                    %build vectors for positive indices
   force_out(i) = force_in(ind(i),2);
   if((ind(i) + index) > length(vel_in))
      vel_out(i) = vel_in(ind(i),2);
   else
      vel_out(i) = vel_in(ind(i) + index,2);
   end
end
```

avals.m

```
%This function calls function 'geta' and uses the returned values to plot
%the best fit curve to represent the FV characteristics for a given applied
%current



a1 = geta(force_0000_ext,vel_0000_ext);     %function call to obtain a values
mean_a1 = mean(medfilt1(a1,500))           %filters the data to remove ambient data
a2 = geta(force_0260_ext,vel_0260_ext);
mean_a2 = mean(medfilt1(a2,500))
a3 = geta(force_0521_ext,vel_0521_ext);
mean_a3 = mean(medfilt1(a3,500))
a4 = geta(force_0781_ext,vel_0781_ext);
mean_a4 = mean(medfilt1(a4,500))
a5 = geta(force_1042_ext,vel_1042_ext);
mean_a5 = mean(medfilt1(a5,500))
a6 = geta(force_1302_ext,vel_1302_ext);
mean_a6 = mean(medfilt1(a6,500))
a7 = geta(force_1563_ext,vel_1563_ext);
mean_a7 = mean(medfilt1(a7,500))
a8 = geta(force_1823_ext,vel_1823_ext);
mean_a8 = mean(medfilt1(a8,500))
a9 = geta(force_2083_ext,vel_2083_ext);
mean_a9 = mean(medfilt1(a9,500))



x = linspace(0,0.06,400);
plot(x,mean_a1.*x.*x);
hold on
axis([-0.04 0.04 -2000 2000]);
plot(x,mean_a2.*x.*x);                  %plots the best fit curve for the FV data at the given
applied current
plot(x,mean_a3.*x.*x);
plot(x,mean_a4.*x.*x);
plot(x,mean_a5.*x.*x);
plot(x,mean_a6.*x.*x);
plot(x,mean_a7.*x.*x);
plot(x,mean_a8.*x.*x);
plot(x,mean_a9.*x.*x);
plot(-x,-mean_a1.*x.*x);
```

```
plot(-x,-mean_a2.*x.*x);
plot(-x,-mean_a3.*x.*x);
plot(-x,-mean_a4.*x.*x);
plot(-x,-mean_a5.*x.*x);
plot(-x,-mean_a6.*x.*x);
plot(-x,-mean_a7.*x.*x);
plot(-x,-mean_a8.*x.*x);
plot(-x,-mean_a9.*x.*x);



% mean_a = [mean_a1 mean_a2 mean_a3 mean_a4 mean_a5 mean_a6 mean_a7
mean_a8 mean_a9];
% x = [0.27 0.36 0.45 0.60 0.84 1.2];
%
% plot(x, mean_a,'.','markersize',20)
%axis([0.2 1.4 0.09 0.18]);
```

geta.m

```
%This function calculates and returns the a value for each of the data
%points within the force and velocity data sets from the applied current
%experiment.


function a = geta(force_in,vel_in)

   for i=1:length(vel_in)
      a(i) = force_in(i)/(vel_in(i)*vel_in(i));   %calculate a from equation f = a*v^2
   end
```

FI_plots.m

```
%This function plots the best fit curve calculated for each of the
%different applied current data sets.  The units of the plot are m vs. N



x = linspace(0,75,500);
plot(x,3.2281*10^5.*x.*x+3000*x+120);
hold on;
axis([-0.06 0.06 -2000 2000]);
plot(x,3.5281*10^5.*x.*x+3000*x+120);
plot(x,3.7281*10^5.*x.*x+1500*x+150);
plot(x,3.8281*10^5.*x.*x+1500*x+170);
plot(x,3.4281*10^5.*x.*x+3500*x+190);
plot(x,3.9281*10^5.*x.*x+3500*x+240);
plot(x,4.1281*10^5.*x.*x+3500*x+320);
plot(x,4.9281*10^5.*x.*x+3500*x+340);
plot(x,5.2281*10^5.*x.*x+4000*x+350);
plot(-x,-3.2281*10^5.*x.*x+3000*x+120);
plot(-x,-3.5281*10^5.*x.*x+3000*x+120);
plot(-x,-3.7281*10^5.*x.*x+1500*x+150);
plot(-x,-3.8281*10^5.*x.*x+1500*x+170);
plot(-x,-3.4281*10^5.*x.*x+3500*x+190);
plot(-x,-3.9281*10^5.*x.*x+3500*x+240);
plot(-x,-4.1281*10^5.*x.*x+3500*x+320);
plot(-x,-4.9281*10^5.*x.*x+3500*x+340);
plot(-x,-5.2281*10^5.*x.*x+4000*x+350);


temp = [3.5281*10^5 3.7281*10^5 3.8281*10^5 3.4281*10^5 3.9281*10^5 4.1281*10^5
4.9281*10^5 5.2281*10^5];
i = [260 521 781 1042 1302 1563 1823 2083];
plot(i,temp,'.')
```

FI_plots_mm.m

```
%This function plots the best fit curve calculated for each of the
%different applied current data sets.  The units of the plot are mm vs. N


x = linspace(0,75,500);
plot(x,0.275.*x.*x+3*x+250, 'b', 'linewidth', 2)
hold on
axis([-70 70 -2000 2000]);
plot(x,0.31.*x.*x+3*x+250, 'b', 'linewidth', 2)
plot(x,0.32.*x.*x+3*x+250, 'b', 'linewidth', 2)
plot(x,0.33.*x.*x+360, 'b', 'linewidth', 2)
plot(x,0.345.*x.*x+360, 'b', 'linewidth', 2)
plot(x,0.375.*x.*x+450, 'b', 'linewidth', 2)
plot(x,0.405.*x.*x+520, 'b', 'linewidth', 2)
plot(x,0.49.*x.*x+520, 'b', 'linewidth', 2)
plot(x,0.52.*x.*x+520, 'b', 'linewidth', 2)
plot(-x,-0.275.*x.*x+3*x+250, 'b', 'linewidth', 2)
plot(-x,-0.31.*x.*x+3*x+250, 'b', 'linewidth', 2)
plot(-x,-0.32.*x.*x+3*x+250, 'b', 'linewidth', 2)
plot(-x,-0.33.*x.*x+360, 'b', 'linewidth', 2)
plot(-x,-0.345.*x.*x+360, 'b', 'linewidth', 2)
plot(-x,-0.375.*x.*x+450, 'b', 'linewidth', 2)
plot(-x,-0.405.*x.*x+520, 'b', 'linewidth', 2)
plot(-x,-0.49.*x.*x+520, 'b', 'linewidth', 2)
plot(-x,-0.52.*x.*x+520, 'b', 'linewidth', 2)
xlabel('Velocity (mm/s)');
ylabel('Force (Newtons)');
```

plotall.m

```
%This function plots all of the force-velocity data for the applied current
%experiment in scatter plot form with different colors representing
%different data sets


index = 6;
plot(vel_0000_ext(3+index:length(vel_0000_ext)),force_0000_ext(3:length(vel_0000_ex
t)-index),'.','markeredgecolor','b');
hold on;
axis([0 70 0 2000]);
pause(1);
plot(vel_0260_ext(3+index:length(vel_0260_ext)),force_0260_ext(3:length(vel_0260_ex
t)-index),'.','markeredgecolor','k');
pause(1);
plot(vel_0521_ext(3+index:length(vel_0521_ext)),force_0521_ext(3:length(vel_0521_ex
t)-index),'.','markeredgecolor','r');
pause(1);
plot(vel_0781_ext(3+index:length(vel_0781_ext)),force_0781_ext(3:length(vel_0781_ex
t)-index),'.','markeredgecolor','g');
pause(1);
plot(vel_1042_ext(3+index:length(vel_1042_ext)),force_1042_ext(3:length(vel_1042_ex
t)-index),'.','markeredgecolor','y');
pause(1);
plot(vel_1302_ext(3+index:length(vel_1302_ext)),force_1302_ext(3:length(vel_1302_ex
t)-index),'.','markeredgecolor','m');
pause(1);
plot(vel_1563_ext(3+index:length(vel_1563_ext)),force_1563_ext(3:length(vel_1563_ex
t)-index),'.','markeredgecolor','b');
pause(1);
plot(vel_1823_ext(3+index:length(vel_1823_ext)),force_1823_ext(3:length(vel_1823_ex
t)-index),'.','markeredgecolor','k');
pause(1);
plot(vel_2083_ext(3+index:length(vel_2083_ext)),force_2083_ext(3:length(vel_2083_ex
t)-index),'.','markeredgecolor','r');
```

separate_extension_plots.m

```
%This function plots the force-velocity characteristics for each of the
%different applied current data sets.  The plots are each in a different
%figure.


figure(1)
index = 6;
plot(vel_0000_ext(3+index:length(vel_0000_ext)),force_0000_ext(3:length(vel_0000_ex
t)-index),'.','markeredgecolor','k');
hold on;
axis([0 70 0 2000]);
plot(x,0.275.*x.*x+3*x+250, 'b', 'linewidth', 2)
xlabel('Velocity (mm/s)');
ylabel('Force (Newtons)');
hold off;

figure(2)
plot(vel_0260_ext(3+index:length(vel_0260_ext)),force_0260_ext(3:length(vel_0260_ex
t)-index),'.','markeredgecolor','k');
hold on;
axis([0 70 0 2000]);
plot(x,0.31.*x.*x+3*x+250, 'b', 'linewidth', 2)
xlabel('Velocity (mm/s)');
ylabel('Force (Newtons)');
hold off

figure(3)
plot(vel_0521_ext(3+index:length(vel_0521_ext)),force_0521_ext(3:length(vel_0521_ex
t)-index),'.','markeredgecolor','k');
hold on;
axis([0 70 0 2000]);
plot(x,0.32.*x.*x+3*x+250, 'b', 'linewidth', 2)
xlabel('Velocity (mm/s)');
ylabel('Force (Newtons)');
hold off

figure(4)
plot(vel_0781_ext(3+index:length(vel_0781_ext)),force_0781_ext(3:length(vel_0781_ex
t)-index),'.','markeredgecolor','k');
hold on;
```

```
axis([0 70 0 2000]);
plot(x,0.33.*x.*x+360, 'b', 'linewidth', 2)
xlabel('Velocity (mm/s)');
ylabel('Force (Newtons)');
hold off

figure(5)
plot(vel_1042_ext(3+index:length(vel_1042_ext)),force_1042_ext(3:length(vel_1042_ex
t)-index),'.','markeredgecolor','k');
hold on;
axis([0 70 0 2000]);
plot(x,0.345.*x.*x+360, 'b', 'linewidth', 2)
xlabel('Velocity (mm/s)');
ylabel('Force (Newtons)');
hold off

figure(6)
plot(vel_1302_ext(3+index:length(vel_1302_ext)),force_1302_ext(3:length(vel_1302_ex
t)-index),'.','markeredgecolor','k');
hold on;
axis([0 70 0 2000]);
plot(x,0.375.*x.*x+450, 'b', 'linewidth', 2)
xlabel('Velocity (mm/s)');
ylabel('Force (Newtons)');
hold off

figure(7)
plot(vel_1563_ext(3+index:length(vel_1563_ext)),force_1563_ext(3:length(vel_1563_ex
t)-index),'.','markeredgecolor','k');
hold on;
axis([0 70 0 2000]);
plot(x,0.405.*x.*x+520, 'b', 'linewidth', 2)
xlabel('Velocity (mm/s)');
ylabel('Force (Newtons)');
hold off

figure(8)
plot(vel_1823_ext(3+index:length(vel_1823_ext)),force_1823_ext(3:length(vel_1823_ex
t)-index),'.','markeredgecolor','k');
hold on;
axis([0 70 0 2000]);
plot(x,0.49.*x.*x+520, 'b', 'linewidth', 2)
xlabel('Velocity (mm/s)');
ylabel('Force (Newtons)');
hold off
```

```
figure(9)
plot(vel_2083_ext(3+index:length(vel_2083_ext)),force_2083_ext(3:length(vel_2083_ex
t)-index),'.','markeredgecolor','k');
hold on;
axis([0 70 0 2000]);
plot(x,0.52.*x.*x+520, 'b', 'linewidth', 2)
xlabel('Velocity (mm/s)');
ylabel('Force (Newtons)');
hold off
```

APPENDIX C

LabVIEW Data Acquisition Code

MagThesis.vi Front Panel

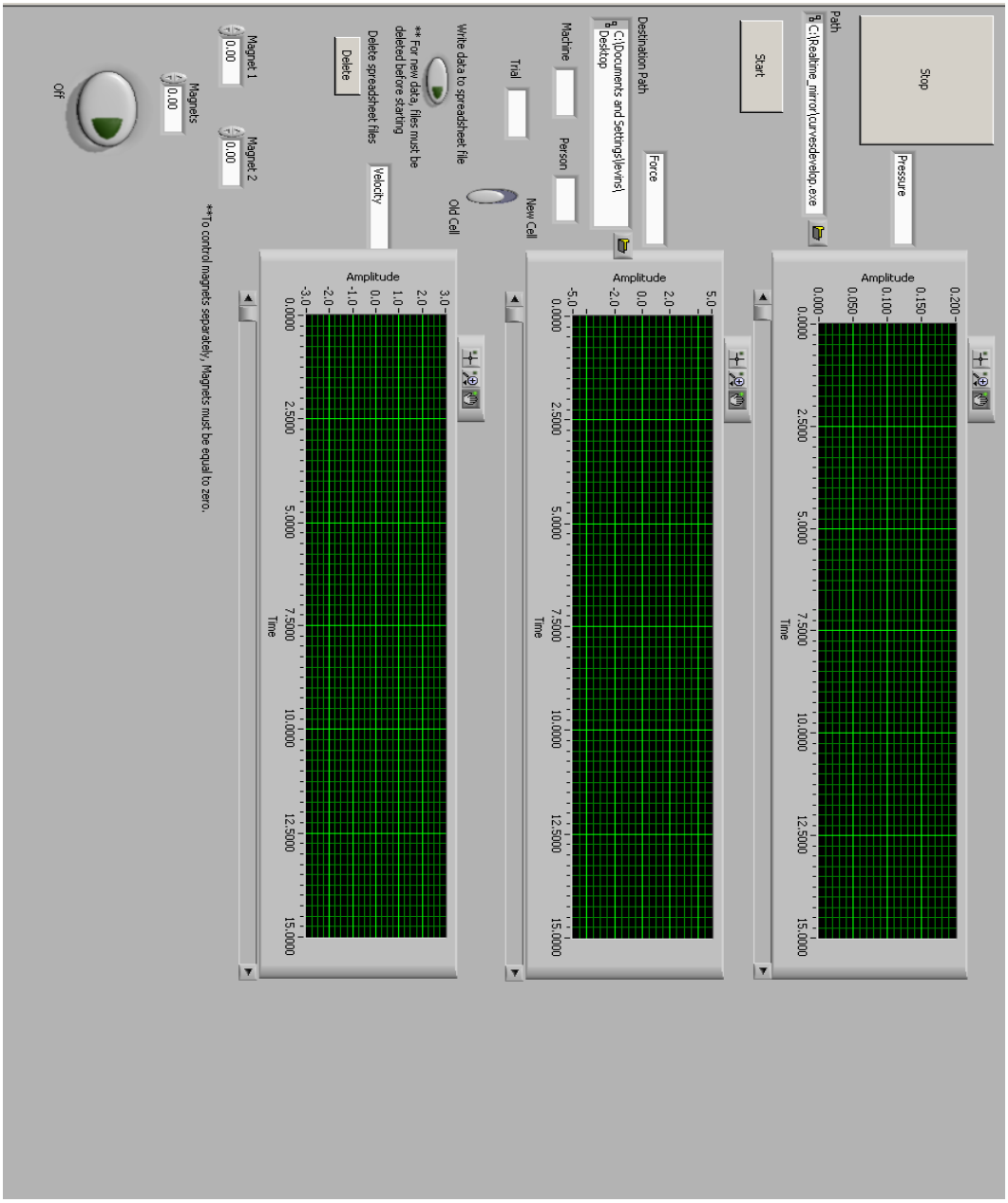

MagThesis.vi Block Diagram

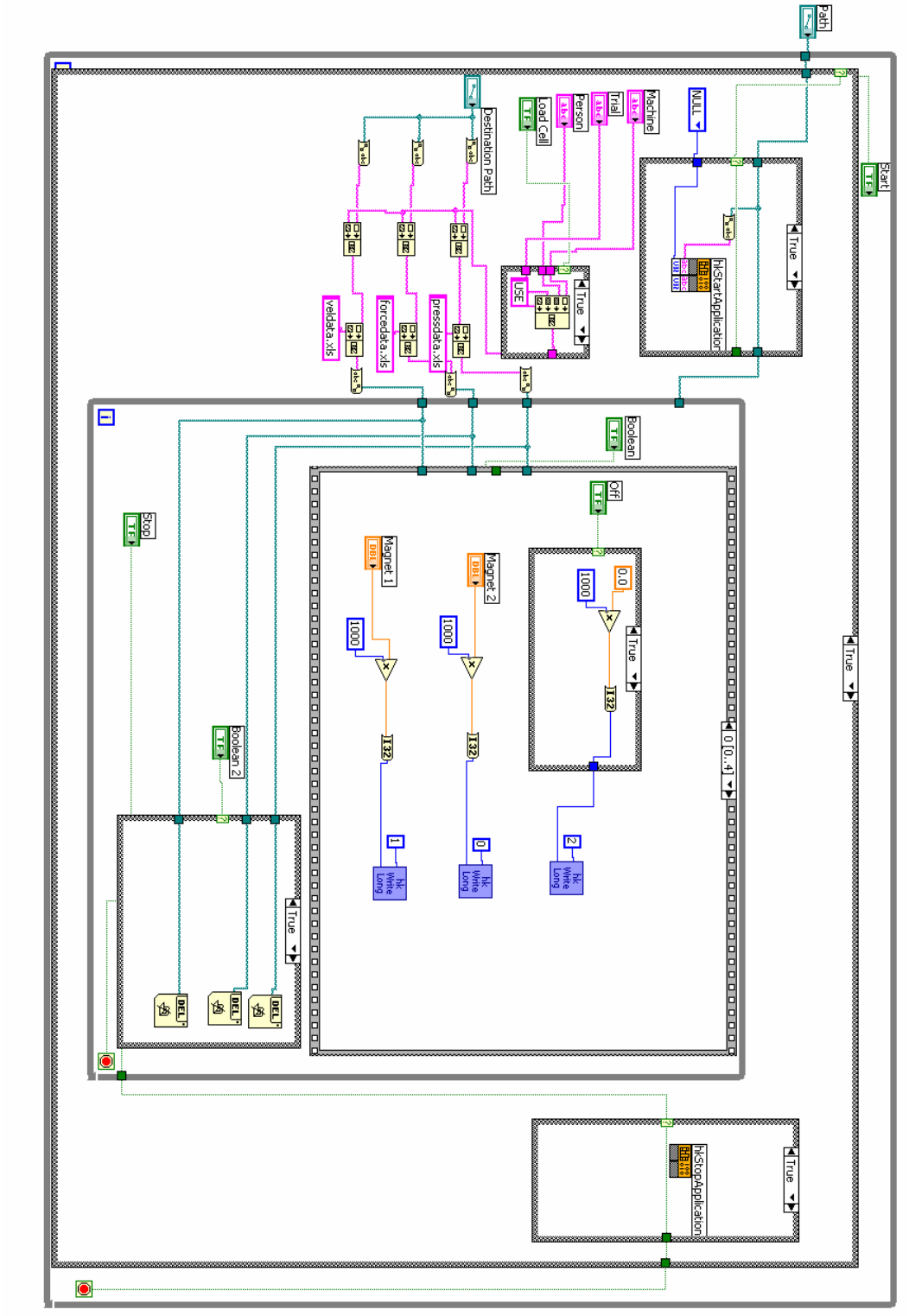

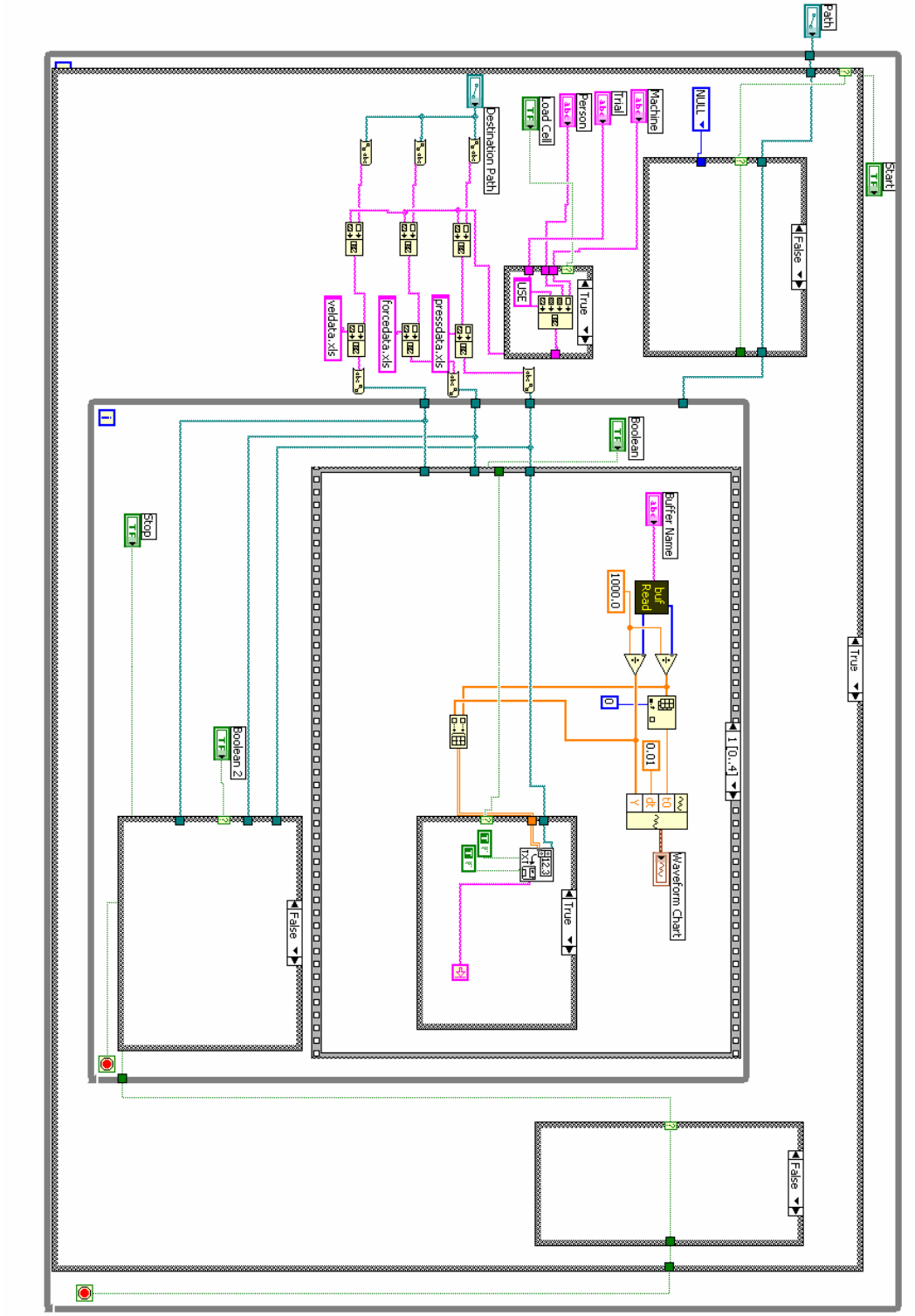
Path
Destination Path
Load Cell
Person
Trial
Machine
NULL
Start
False
USE
True
veldata.xls
forcedata.xls
pressdata.xls
Boolean
Stop
Buffer Name
1000.0
buf Read
Boolean 2
0.01
1 [0..4]
Waveform Chart
True
False
False

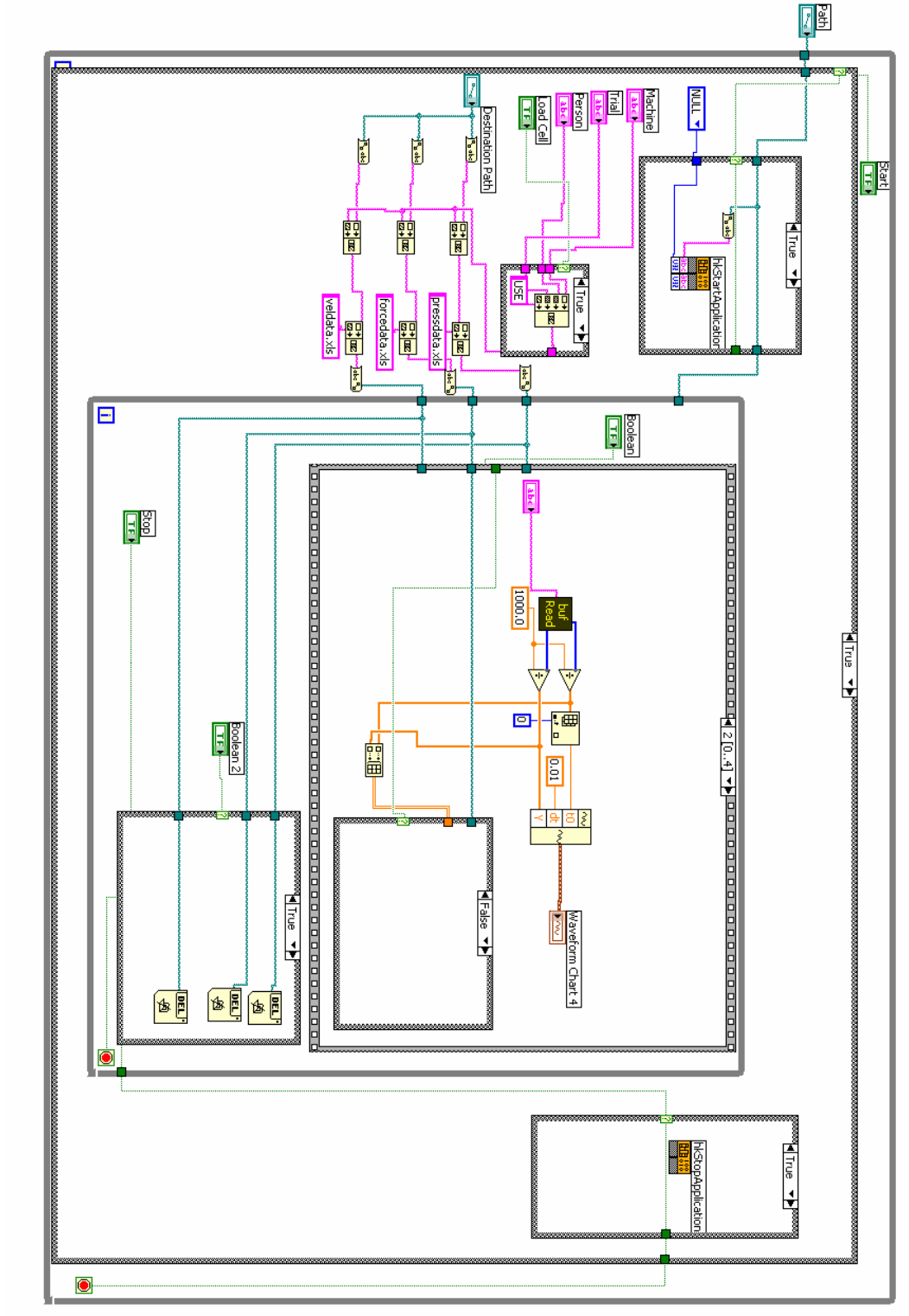
Path
Start
Destination Path
Load Cell
Person
Trial
Machine
NULL
True
hkStartApplication
USE
True
veldata.xls
forcedata.xls
pressdata.xls
Boolean
Stop
1000.0
buf Read
0
0.01
2 [0..4]
Boolean 2
True
DEL
False
Waveform Chart 4
True
hkStopApplication

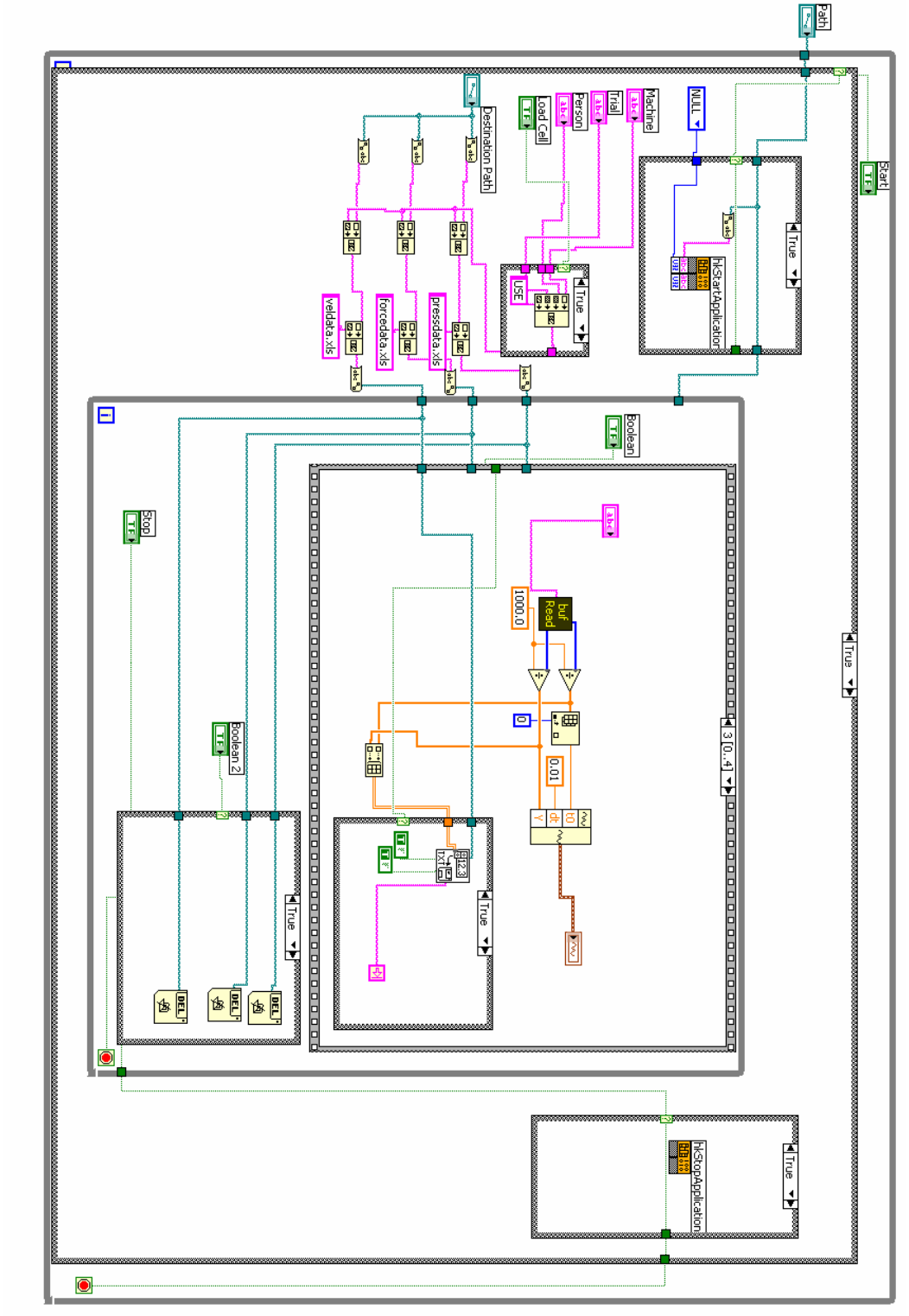
Path
Destination Path
Load Cell
Person
Trial
Machine
NULL
Start
True
hkStartApplication
USE
True
veldata.xls
forcedata.xls
pressdata.xls
Boolean
Stop
1000.0
buf Read
0
0.01
3 [0..4]
Boolean 2
True
DEL
DEL
DEL
True
Truu
hkStopApplication
True

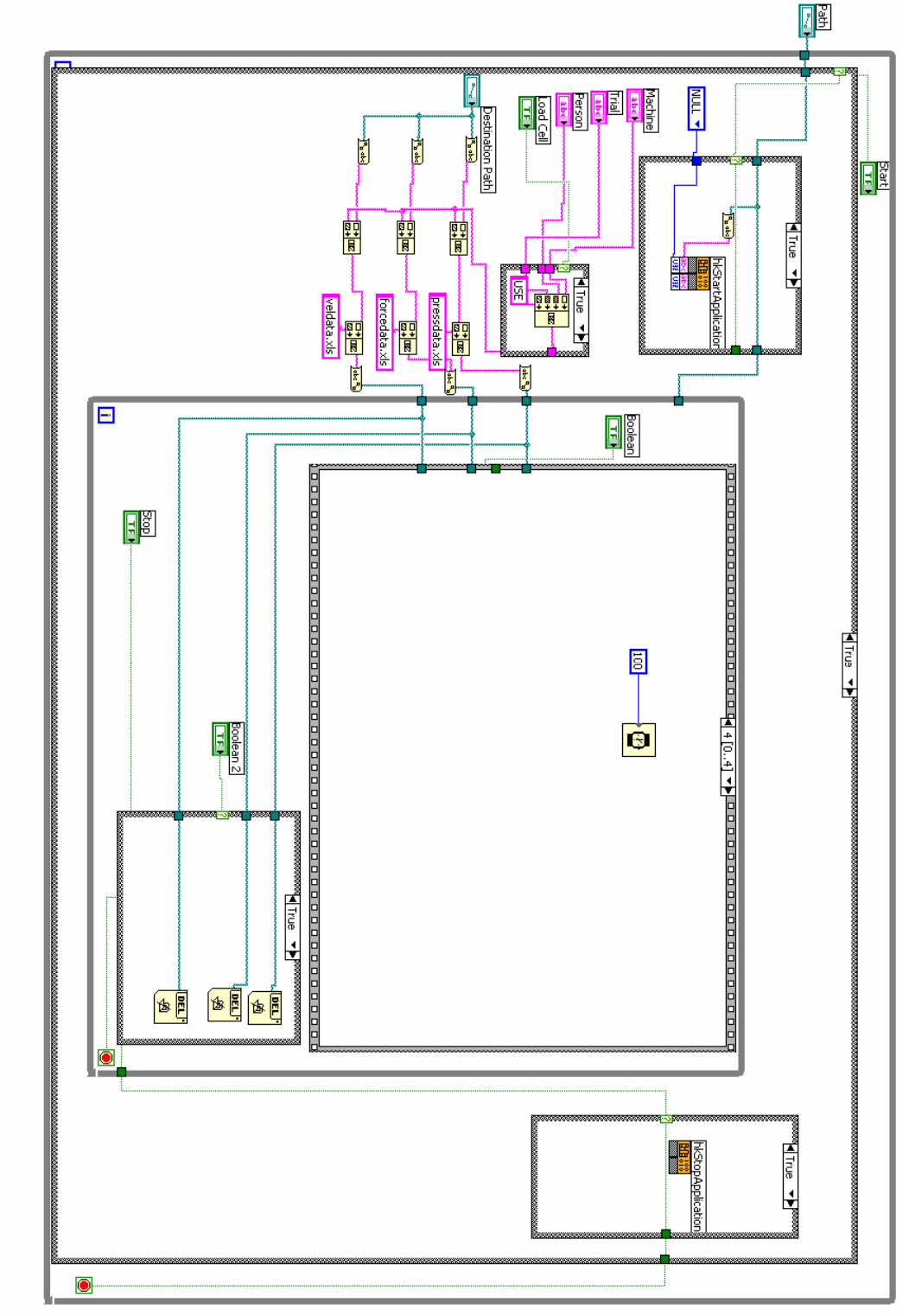
Path
Destination Path
Load Cell
Person
Trial
Machine
NULL
Start
True
hkStartApplication
USE
True
veldata.xls
forcedata.xls
pressdata.xls
Boolean
Stop
Boolean 2
100
4 [0..4]
True
DEL
DEL
DEL
True
hkStopApplication
True

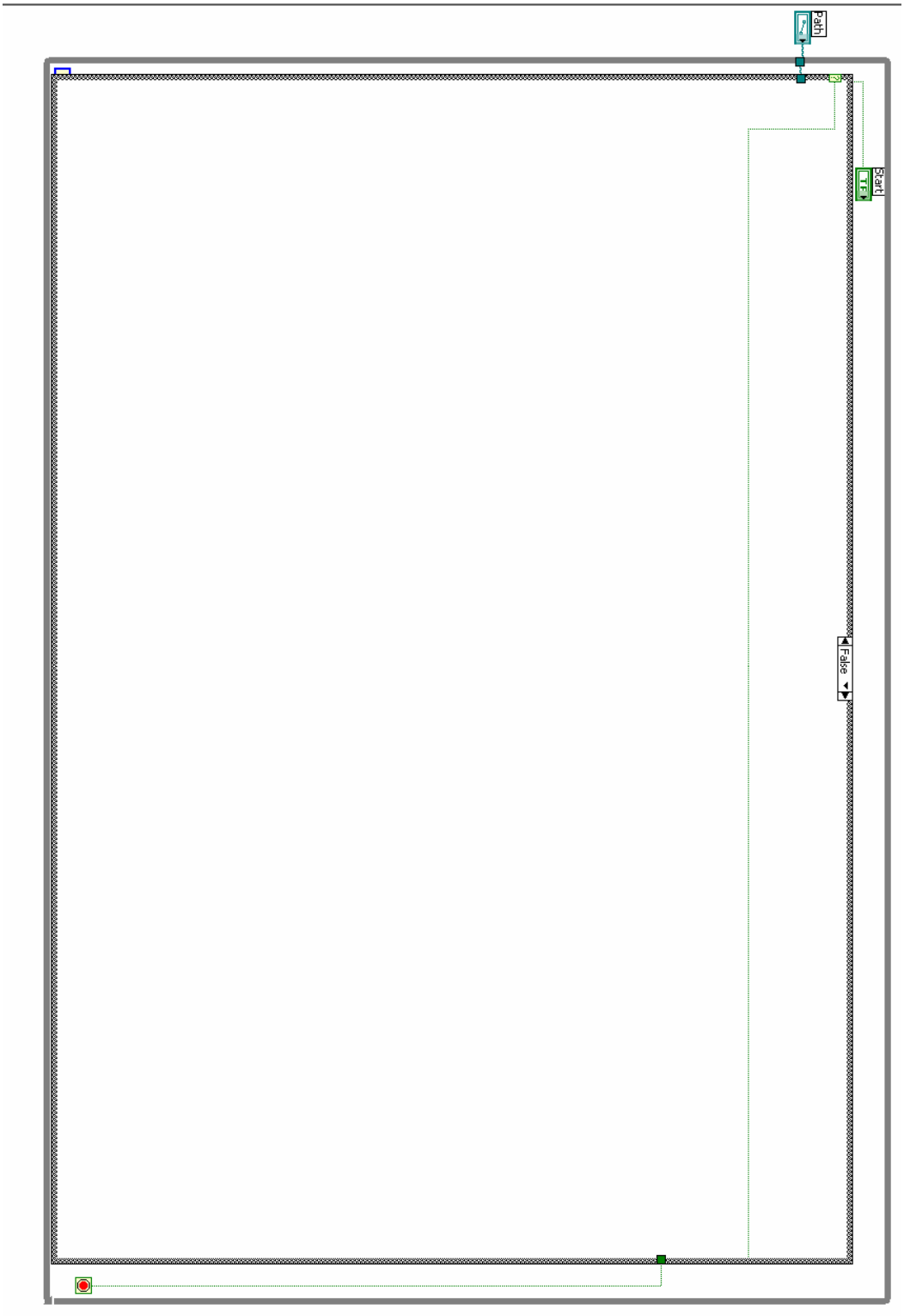
Path
Start
False

hkWriteLong.vi Front Panel

hkWriteLong.vi Block Diagraml

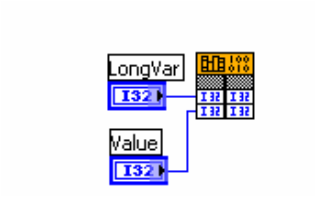

APPENDIX D

HyperKernel C Code

CurvesDevelop.c

```
// Curvesdevelop.C                    Ian Gravagne, Brett Levins 3/17/04, Baylor University
//
// A linear displacement and velocity test routine.

#include <hKernel.h>
#include "C:\Documents and Settings\levins\Desktop\Realtime\\stgdriver\\stgdriver.h"
#include "C:\Documents and Settings\levins\Desktop\Realtime\\databuffer\\databuffer.h"


void analog_in_thread(void);
void analog_in_thread_ISR(void);
long analog_in_thread_ID;
long *buffer;
long *buffer2;
long *buffer3;

double low_bound(double);
double g(double a, double b);
double signum(double);

void main(void)
{

        double zero[] = {0.0,0.0,0.0,0.0,0.0,0.0,0.0,0.0};
        double ain[8];

        // Print some instructions
        hkPrint("");
        hkPrint("----------------------");
        hkPrint("Linear Displacement and Velocity Reading System (Ian Gravagne, Brett Levins, 2004)");
        hkPrint("----------------------");
        hkPrint("");

        // Do some initialization
        stgSetBaseAddress(0x300);
```

```
	stgAnalogCalibrate();
	stgAnalogAllOut(zero);
	stgInitEncoders();
	stgSetPortDirection(STG_PORT_A, OUTPUT);
	buffer  = bufCreate("Position", 2000);
	buffer2 = bufCreate("Velocity", 2000);
	buffer3 = bufCreate("Force", 2000);

	// Start ADC waveform thread and attach the timer ISR
	analog_in_thread_ID = hkCreateThread(analog_in_thread, MIN_STACK_SIZE,
"analog_in", 28);
	hkAttachSystemTimer(analog_in_thread_ISR, NULL);

	// Loop until stopped...
	while(!hkQuitRequest())
	{
		// Read state of ADC channels
		stgAnalogAllIn(ain);

		// delay for a while
		hkSleep(100);

	}

	// cleanup, and zero out the DACs
	hkDetachSystemTimer(analog_in_thread_ISR);
	hkKillThread(analog_in_thread_ID);
	stgAnalogAllOut(zero);
	stgDigitalAllOut(0x00);
	bufDestroy("Position");
	bufDestroy("Velocity");
	bufDestroy("Force");
}


void analog_in_thread(void)
{
	long i = 0;			// sample counter
	long j = 0;			// timer counter
	long k = 0;
	int count = 0;
	int state = 0;
	int angle = 0;
	int flag;

	double x = 0.0;
```

```
double fs = 1000.0;     // sampling frequency
double force;
double pressure, pressurea, pressureb;
double position, position2 = 0.0, position3 = 0.0, position4 = 0.0, position5 = 0.0;
double velocity, velocity2 = 0.0, velocity3 = 0.0, velocity4 = 0.0, velocity5 = 0.0;
double accel, accel2 = 0.0, accel3 = 0.0, accel4 = 0.0, accel5 = 0.0;
double heartrate;
double currenti = 0.0, currenti2 = 0.0, currenti3 = 0.0, currenti4 = 0.0;
double currento = 0.0, currento2 = 0.0, currento3 = 0.0, currento4 = 0.0;
double voltage;
double magnet1, magnet2, magnets;
double MA;
double dir=0;

while(1)
{
        if(hkReceive(ANYTID,NULL,0) == SIGNALED)
        {

                if(j%20 == 0)
                {
                        i++;

                        magnet1 = (double)hkReadLong(1)/1000.0;
                        magnet2 = (double)hkReadLong(0)/1000.0;
                        magnets = (double)hkReadLong(2)/1000.0;


                        if (magnets > 0.01){
                                stgAnalogOut(0,magnets);
                                stgAnalogOut(1,magnets);
                        }
                        else if (magnets < 0.01){
                                stgAnalogOut(0,magnet1);
                                stgAnalogOut(1,magnet2);
                        }
                        else{
                                stgAnalogOut(0,0.0);
                                stgAnalogOut(1,0.0);
                        }


                        position = -(long)stgReadEncoder(0)/205.0;
```

```
                                force = stgAnalogIn(1);

                                velocity = 1.4816*velocity2 - 0.5488*velocity3 +
6.6674*position2 - 6.6674*position3;

                                accel = 1.4816*accel2 - 0.5488*accel3 + 6.6674*velocity2
- 6.6674*velocity3;

                                position5 = position4;position4 = position3;position3 =
position2;position2 = position;
                                velocity5 = velocity4;velocity4 = velocity3;velocity3 =
velocity2;velocity2 = velocity;
                                accel5 = accel4; accel4 = accel3; accel3 = accel2; accel2 =
accel;




                                bufAddPoint(buffer,  i*(long)(1000.0*.01),
(long)(1000.0*position));
                                bufAddPoint(buffer2, i*(long)(1000.0*.01),
(long)(1000.0*(velocity)));
                                bufAddPoint(buffer3, i*(long)(1000.0*.01),
(long)(1000.0*(force + 0.425)));

                        }

                        j++;
                        k++;

                }
        }
}


void analog_in_thread_ISR(void)
{
        hkSignal(analog_in_thread_ID);
}

double low_bound(double in)
{
        if(in > 0.0)
                return(in);
        else
```

```
		return(0.0);
}

double g(double a, double b)
{
	if(fabs(a) > fabs(b))
		return(fabs(a-b));
	else
		return(0.0);
}

double signum(double in)
{
	if(in >= 0.0)
		return(1.0);
	else
		return(-1.0);
}
```

APPENDIX E

Force-Velocity Data for Gap Experiment

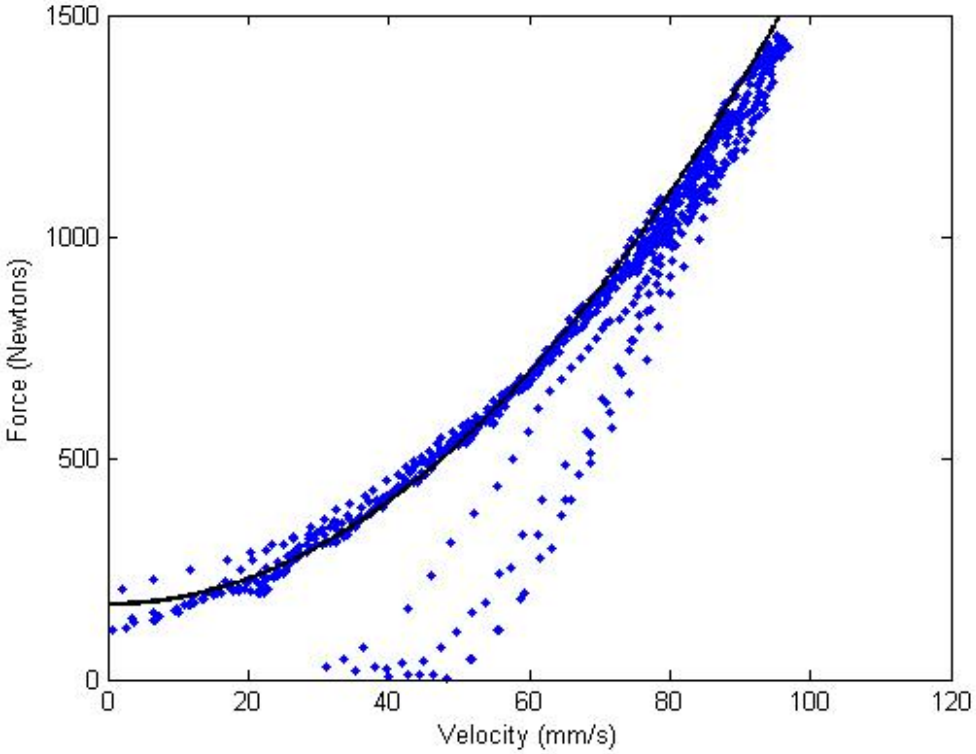

Gap = 0.27mm

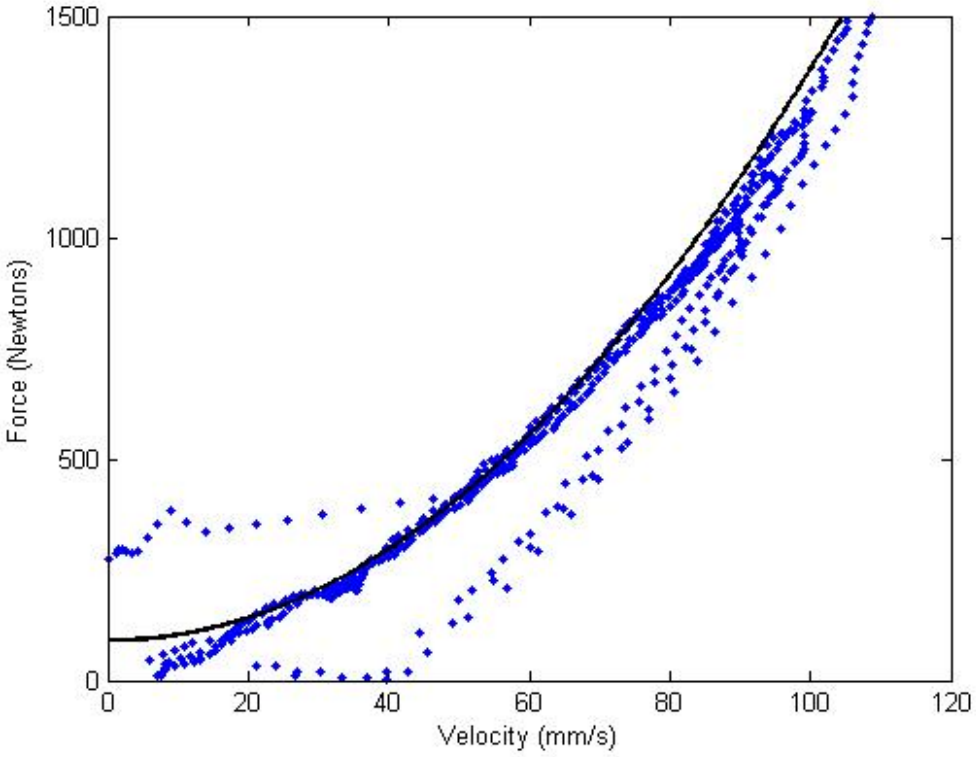

Gap = 0.36mm

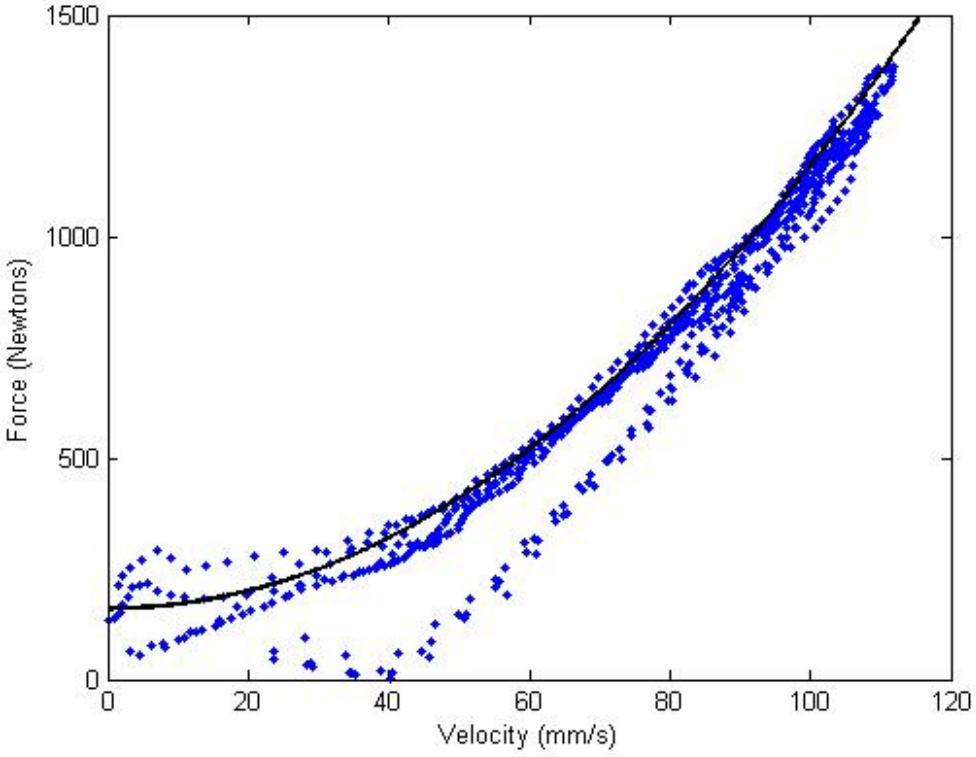

Gap = 0.45mm

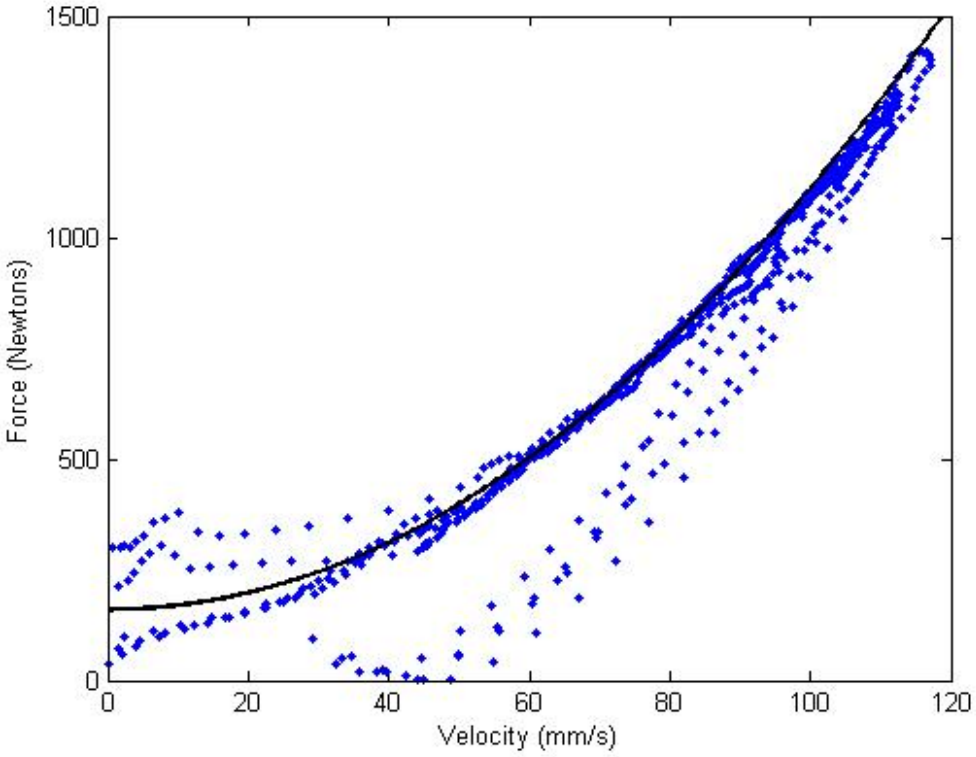

Gap = 0.60mm

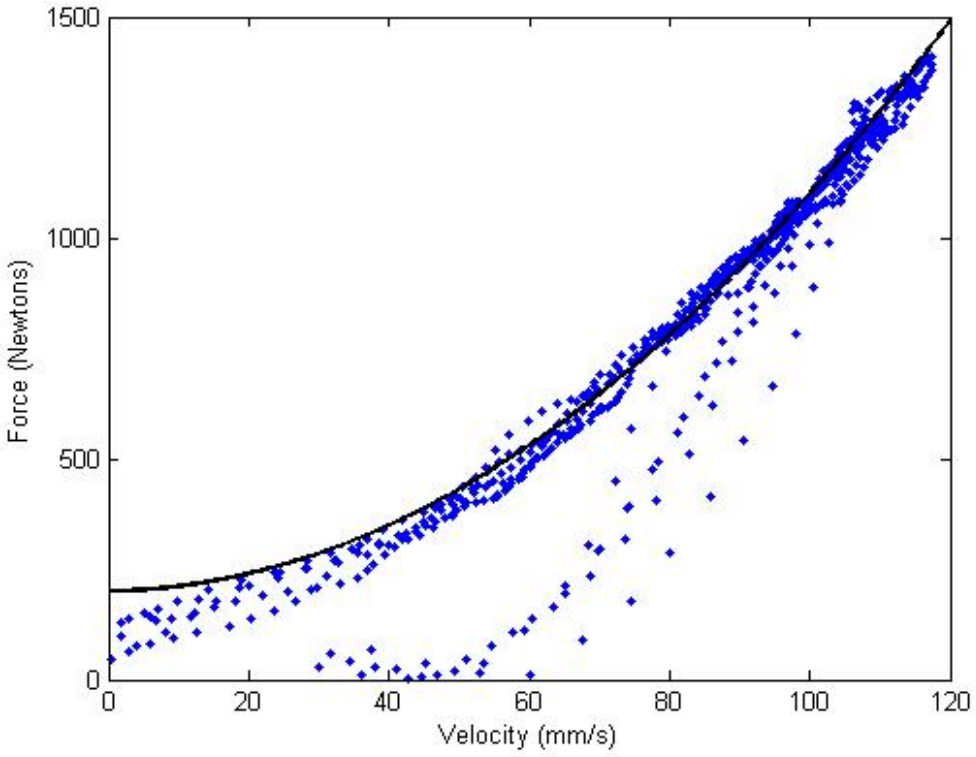

Gap = 0.84mm

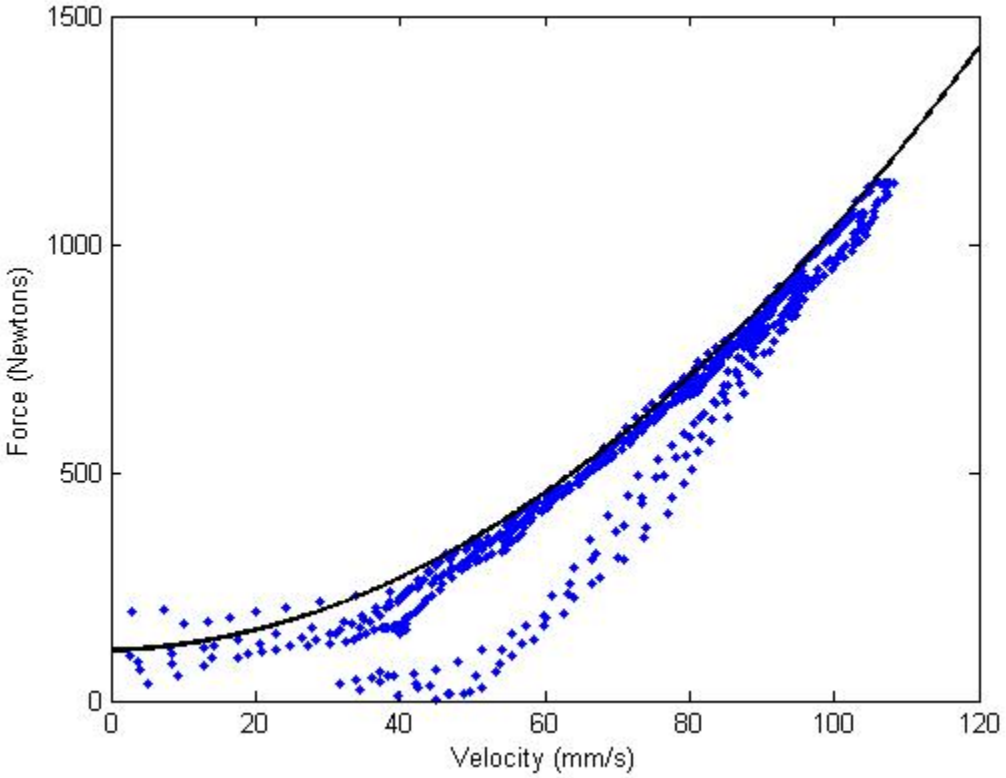
1500
1000
500
0
Force (Newtons)
0
20
40
60
80
100
120
Velocity (mm/s)

Gap = 1.20mm

APPENDIX F

Force-Velocity Data for Applied Current Experiment

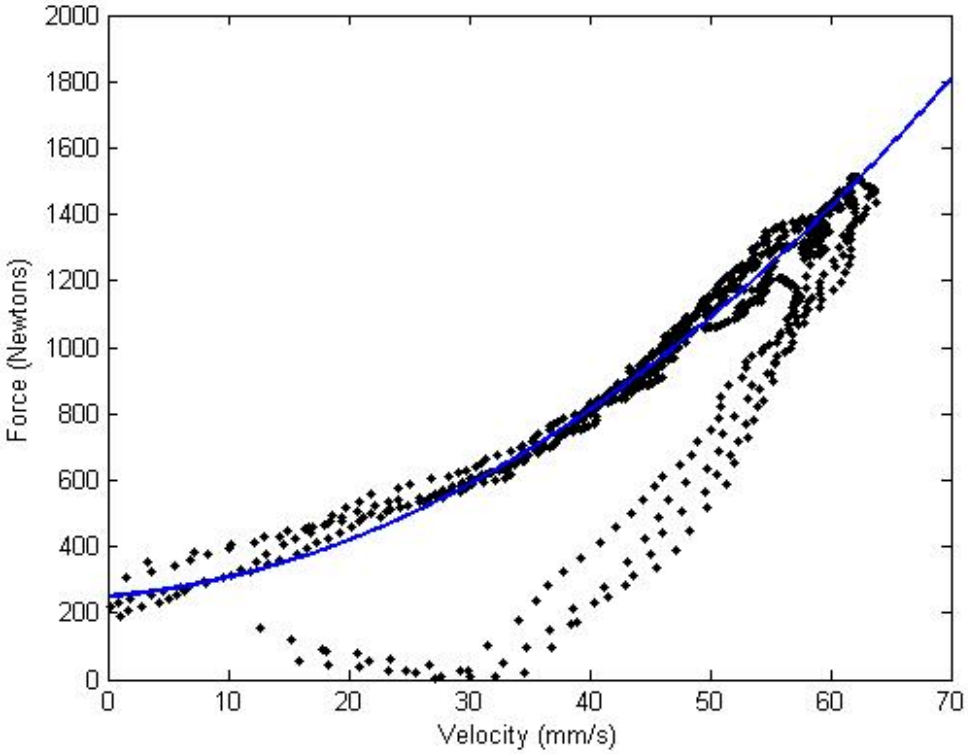

Applied Current = 0.0A

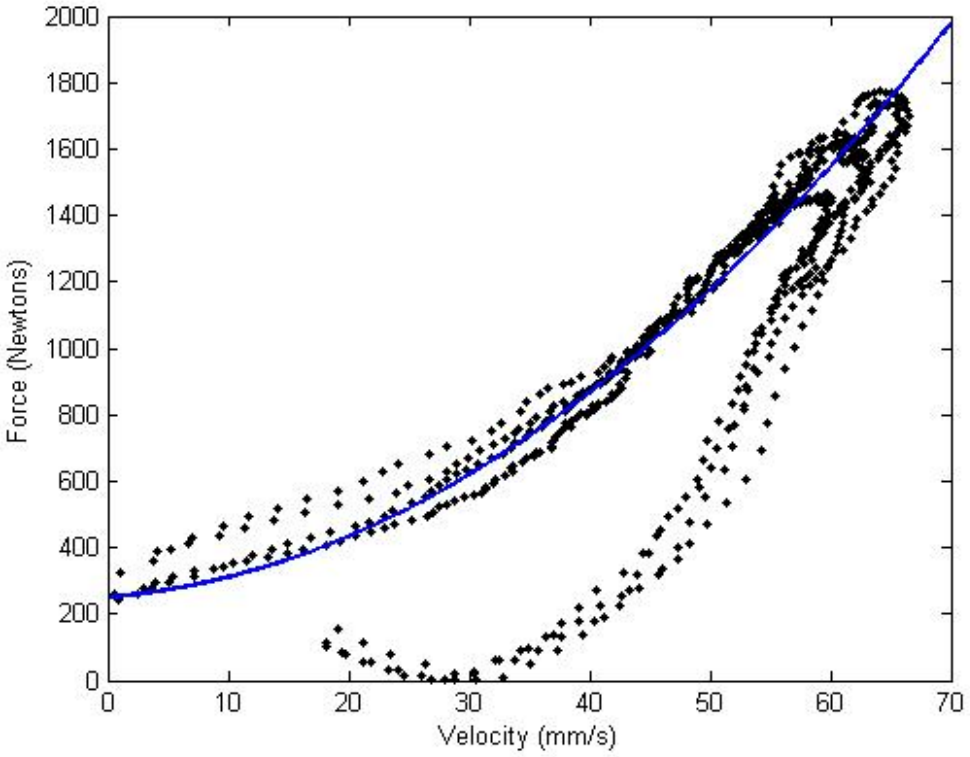

Applied Current = 0.260A

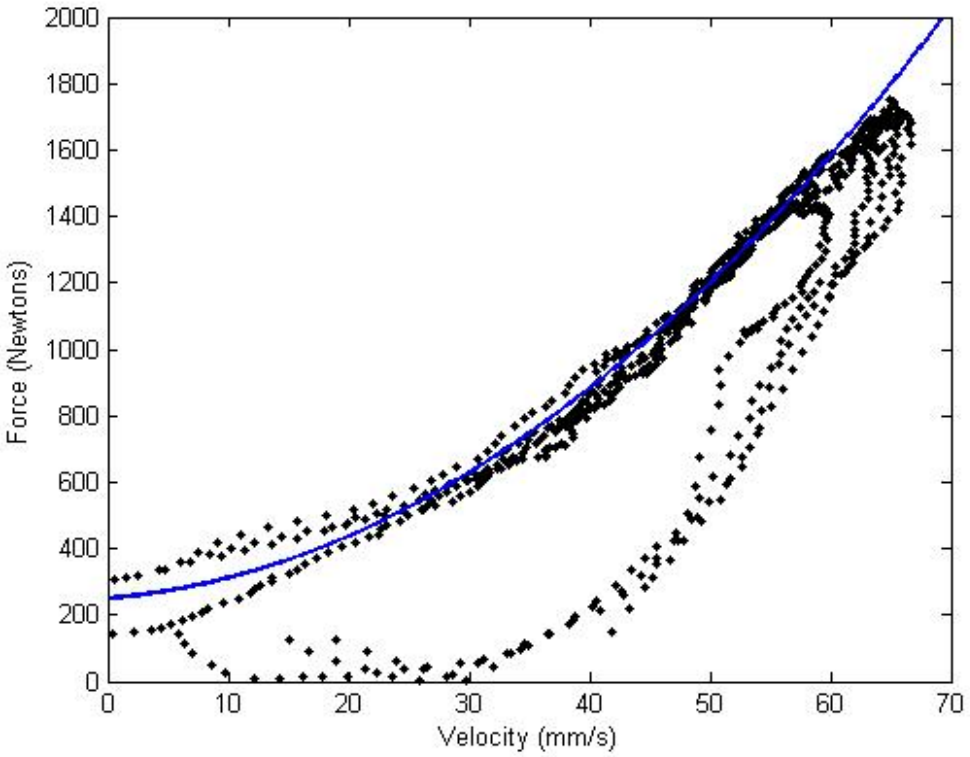

Applied Current = 0.521A

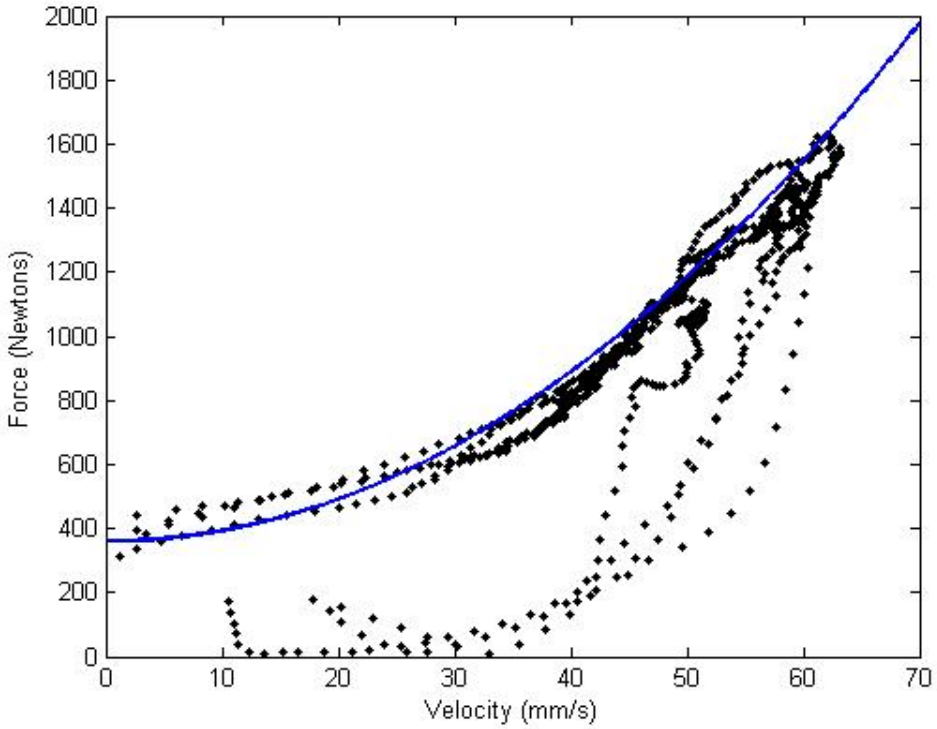

Applied Current = 0.781A

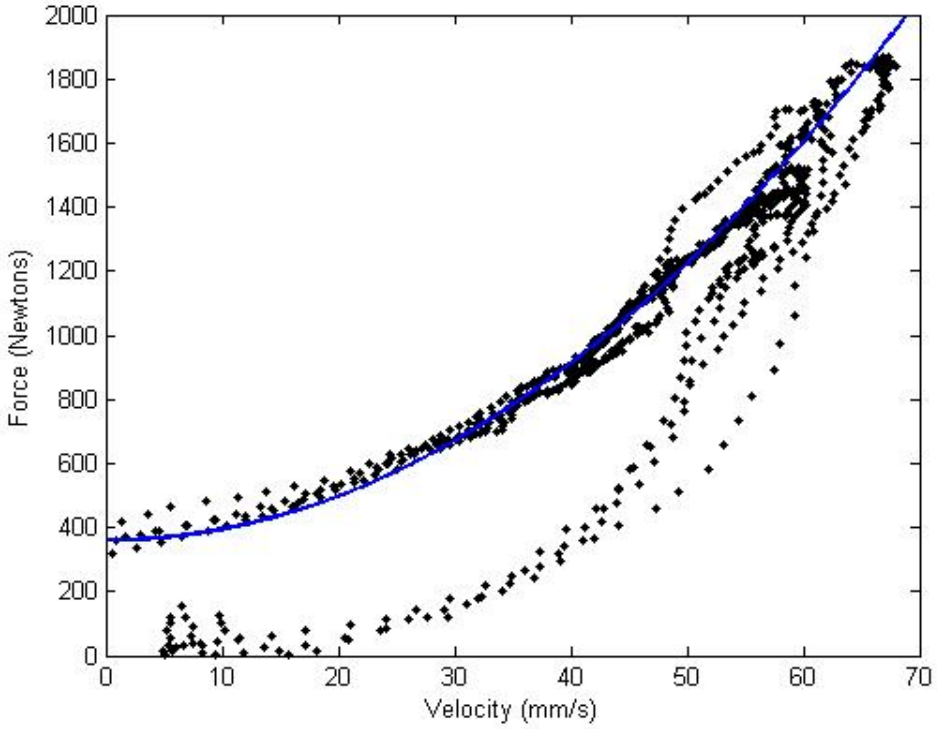

Applied Current = 1.302A

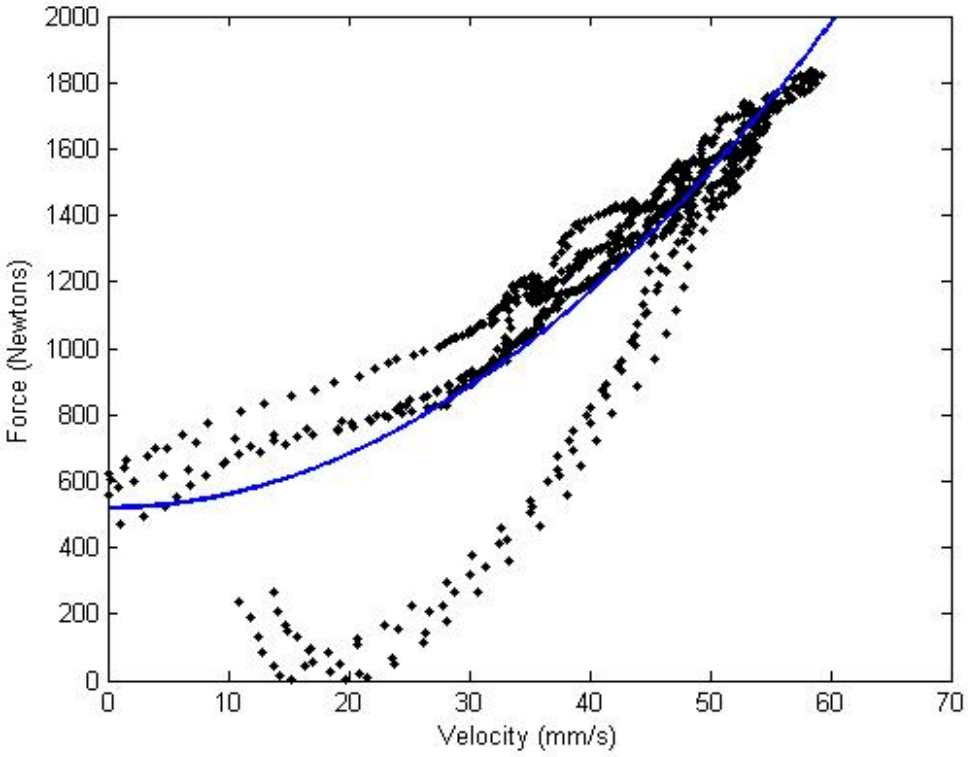

Applied Current = 1.563A

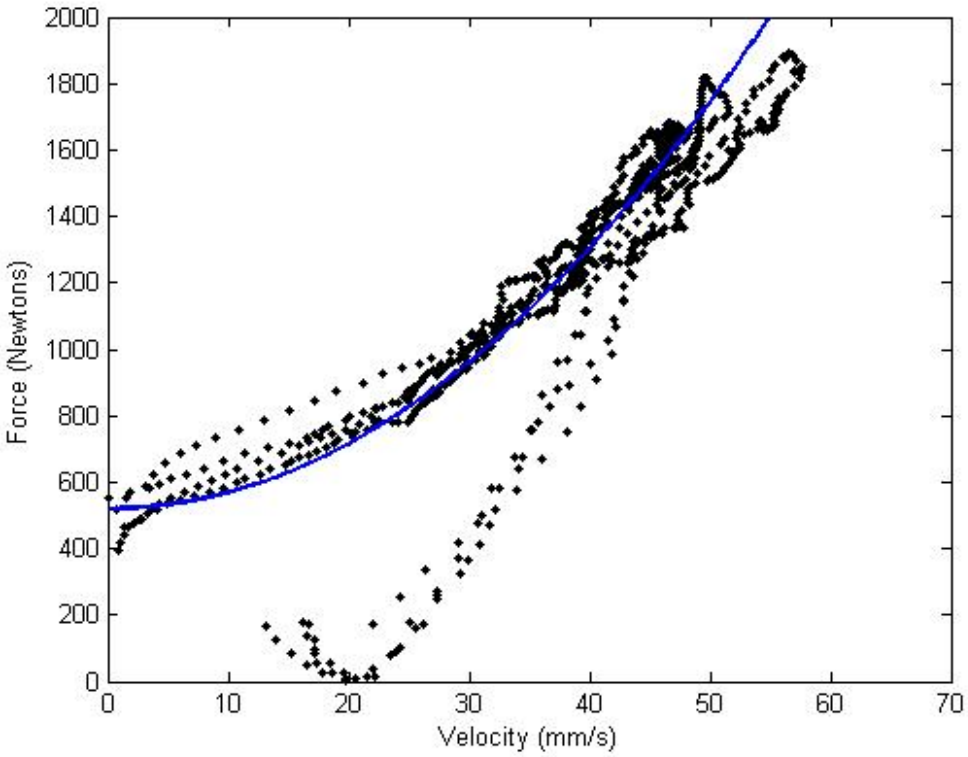

Applied Current = 1.823A

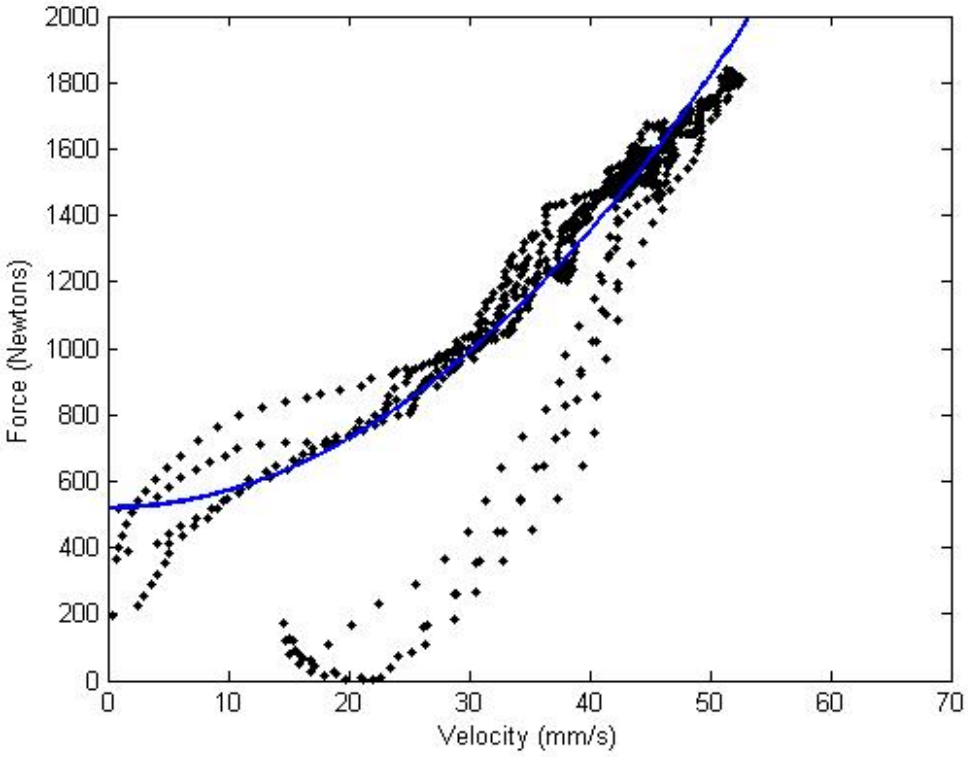
Force (Newtons)
Velocity (mm/s)
0
200
400
600
800
1000
1200
1400
1600
1800
2000
0
10
20
30
40
50
60
70

BIBLIOGRAPHY

[1] D. Carlson, D.M. Catanazarite, K.A. St. Claire, “Commercial magneto-rheological fluid devices,” Proce. 5th Int. Conf. On ER Fluids, MR Suspensions and Assoc. Tech., Singapore, 1996, pp. 20-28.

[2] M.J. Chrzan, J.D. Carlson, “MR fluid sponge devices and their use in vibration control of washing machines,” 8th Annual SPIE Symp. Smart Structures and Materials, Newport Beach, CA, March 2001, pp. 370-378.

[3] J.C. Dixon, The Shock Absorber Handbook, pub. Sept. 1999, Society of Automotive Engineers.

[4] M.R. Jolly, J.W. Bender, J.D. Carlson, “Properties and applications of commercial magnetorheological fluids,” J. Intelligent Material Systems and Structures, vol. 10, no. 1, Jan 2000, pp. 5-13.

[5] Y.B. Kim, W.G. Hwang, C.D. Kee, H.B. Yi, “Active vibration control of a suspension system using an electromagnet damper,” Proc. Instn. Mech. Engrs, vol 215, Part D, pp. 865-873.

[6] J.E. Lindler, Y.T. Choi, N.M. Wereley, “Double adjustable shock absorbers utilizing electrorheological and magnetorheological fluids,” Int. J. Vehicle Design, vol. 33, no. 1-3, pp. 189-206.

[7] A. Lukianovich, O. Ashour, W. Thurston, C. Rogers, “Electrically-controlled adjustable-resistance exercise equipment employing magnetorheological fluid,” Proc. Soc. Photo-optical and Instrumentation Engrs, vol. 2721, pp. 283-291.

[8] D.J. Purdy, “Theoretical and experimental investigation into an adjustable automotive damper,” Proc. Instn. Mech. Engrs, vol. 214, Part D, pp. 265-283.

[9] Y. Suda, T. Shiba, et. al., “Study on electromagnetic damper for automobiles with nonlinear damping force characteristics,” Vehicle System Dynamics Supplement, vol. 41, 2004, pp. 637-646.

[10] LORD Materials Division, “What is the Difference between MR and ER Fluid?,” Presentation, www.lord.com, May 2002.

[11] J. David Carlson, “What makes a good MR Fluid?,” 8th Int. Conf. On Electrorheological (ER) and Magnetorheological (MR) Suspensions, Nice, July 19-13, 2001.

[12] B. Levins, I. Gravagne, “A Magnetically Controllable Valve to Vary the Resistance of Hydraulic Dampers for Exercise Equipment,” to appear, Proc. Int. Conf. on Advanced Intelligent Mechatronics (AIM), Monterey, CA, July 2005.